University of Southern Queensland

Faculty of Engineering & Surveying

Numerical Simulation of Water Waves in Reservoirs Affecting Evaporation

A dissertation submitted by

Edward Stephen Greig

in fulfilment of the requirements of

ENG4111 / ENG4112 Research Project

towards the degree of

Bachelor of Engineering (Civil)

Submitted: January, 2013

Abstract

Predicted increases in evaporation rates from open water reservoirs will likely present sustainability challenges for reservoir dependent communities and industries in the next 50 years. Chemical monolayers have had highly variable success in reducing evaporation rates due breakup and transport by wind-wave action. The effect of wind-wave stretching action on monolayers has not been quantified in the literature. The project aim was to develop a preliminary Computational Fluid Dynamics (CFD) model to determine the average instantaneous shear stresses under wind-wave loadings corresponding to observed monolayer performance limits. Wind speeds of 0.89 m/s and 7.33 m/s are considered representative of the lower and upper limits of degraded monolayer performance. ANSYS Fluent was used to develop a preliminary model, comprising a horizontal tank 15 m long by 0.85 m high with water occupying the bottom half. A constant uniform velocity wind profile was applied to the air inlet for up to five increments of the residence time of three wind speeds, 0.89 m/s, 4.11 m/s and 7.33 m/s. The volume of fluid method was used to capture the movement of the air/water interface. Velocity gradients were extracted from the flow fields and following a one-way analysis of variance test, the average instantaneous shear stresses were determined to be of 0 Pa, 0.00046 Pa and 0.00058 Pa for the increasing wind speeds. These results agree with the expectation that the instantaneous shear stress would increase with increasing wind speed. Significant limitations for the preliminary model include insufficient run time and a lack of average instantaneous shear stress validation. Although this study was limited in scope, there is significant potential for model development which will assist in understanding how monolayers are affected by wind waves, and estimating and improving the operational performance of monolayers in reducing evaporation rates from open water reservoirs.

University of Southern Queensland

Faculty of Engineering and Surveying

ENG4111/2 *Research Project*

Limitations of Use

The Council of the University of Southern Queensland, its Faculty of Engineering and Surveying, and the staff of the University of Southern Queensland, do not accept any responsibility for the truth, accuracy or completeness of material contained within or associated with this dissertation.

Persons using all or any part of this material do so at their own risk, and not at the risk of the Council of the University of Southern Queensland, its Faculty of Engineering and Surveying or the staff of the University of Southern Queensland.

This dissertation reports an educational exercise and has no purpose or validity beyond this exercise. The sole purpose of the course pair entitled "Research Project" is to contribute to the overall education within the student's chosen degree program. This document, the associated hardware, software, drawings, and other material set out in the associated appendices should not be used for any other purpose: if they are so used, it is entirely at the risk of the user.

Prof F Bullen

Dean

Faculty of Engineering and Surveying

Certification of Dissertation

I certify that the ideas, designs and experimental work, results, analyses and conclusions set out in this dissertation are entirely my own effort, except where otherwise indicated and acknowledged.
I further certify that the work is original and has not been previously submitted for assessment in any other course or institution, except where specifically stated.

Edward Stephen Greig

0050014851

_____

Signature

_____

Date

Acknowledgments

I would like to thank Dr Andrew Wandel for his supervision, patience and guidance whilst undertaking this research project. Discussions with him were always comprehensive and enjoyable. His knowledge and experience in computational fluid dynamics, statistical analysis and all matters research related was invaluable.

I would also like to thank management and my colleagues at Tumut Shire Council for their encouragement and support.

Finally, I would like to thank my family and friends for their support, tolerance and encouragement, without which the completion of this dissertation would not have been possible.

This dissertation has been prepared using the USQ LaTeX template.

Edward Stephen Greig

University of Southern Queensland

January 2013

Contents

List of Figures

List of Tables

Nomenclature

a	linear wave amplitude, highest point is a crest, lowest point is a trough (m)
$C = \frac{\omega}{k} = \frac{L}{T}$	wave speed, also known as wave celerity $\left(\mathrm{m.s^{-1}}\right)$
η	surface deviation from the mean still water level (m)
f_x, f_y	body forces (N)
F	volume fraction of a fluid phase
g	gravitational acceleration $\left(\mathrm{m.s^{-2}}\right)$
h	depth of water body (m)
H	wave height, the distance between a wave crest and trough (m)
k_w	wave number $\left(\mathrm{m^{-1}}\right)$
k	turbulent kinetic energy $\left(\mathrm{m^2.s^{-2}}\right)$
L	wave length, the distance between two identical points on successive waves (m)
L_{tank}	length of tank (m)
. λ	second viscosity (Pa.s)
ν	kinematic viscosity $\left(\mathrm{m^2.s^{-1}}\right)$
ω	angular wave frequency $\left(\mathrm{s^{-1}}\right)$
p	pressure (Pa)
$\overline{p}$	mean pressure (Pa)

ρ	fluid density $\left(\text{kg.m}^{-3}\right)$
t	time (s)
T	wave period, time between two successive crests arriving at a point (s)
u, v	velocity vector components $\left(\text{m.s}^{-1}\right)$
u', v'	fluctuating velocity vector components $\left(\text{m.s}^{-1}\right)$
$\overline{u}, \overline{v}$	mean velocity vector components $\left(\text{m.s}^{-1}\right)$
$\mathbf{V}$	two dimensional velocity vector $u\mathbf{i} + v\mathbf{j}$ $\left(\text{m.s}^{-1}\right)$
μ	dynamic viscosity (Pa.s)
μ_T	turbulent viscosity (Pa.s)
x	direction of wave propagation
$z = 0$	still (mean) water level (x-axis)
$z = -h$	bottom of water body

Chapter 1

Introduction

Predicted increases in evaporation rates from open water reservoirs in Australia will present significant sustainability challenges in the coming years for communities and industries which depend upon these storages. Chemical monolayers are a mitigation technique with highly variable success in reducing evaporation rates. This variability is primarily due to breakup and transport of the monolayer by wind-waves. Computational Fluid Dynamics (CFD) is used to investigate the average instantaneous shear stress at the water surface resulting from wind-waves in open reservoirs corresponding to observed monolayer performance limits. This study will complement existing literature and will assist in understanding ad improving monolayer operational performance on open water reservoirs.

Chapter 1 provides an overview of this dissertation. The topics addressed include background, project objectives and scope, a methodology summary, project contributions and a dissertation outline.

1.1 Background

Climate Change predictions in Australia estimate a worst case scenario increase in average temperatures of 5°C and a reduction in rainfall frequency of 50% by 2070 (CSIRO 2007). For regional communities and industries which are dependent of water

storage in open reservoirs, this may present sustainability challenges. There is a need to minimise evaporation rates and to conserve the water already captured in reservoirs. Numerous evaporation mitigation techniques have been investigated over the previous decade, and earlier. These mitigation techniques included the use of wind breaks, destratification techniques, fixed covers and chemical monolayers (Helfer et al. 2011, McJannet et al. 2008). For all but the smallest of reservoirs, chemical monolayers are the only approach considered to be economically feasible. This seems reasonable as the cost of fixed structures would likely be very high and the effects of edge trees in reducing wind action would be minimal for large reservoirs. Although evaporation reductions in the short term may not be appreciable, over an extended term, it is suggested that significant savings may be achieved (Palada, Schouten & Lemckert 2012).

Chemical monolayers are one molecule thick films which spread spontaneously on a water surface and form a barrier to the passage of eater molecules from a water storage into the atmosphere (Barnes 2008). Of the many problems with monolayers in practice, the most significant are breakup and transport by wind and decomposition by microorganisms. Breakup and transport by wind accounts for the highly variable performance results in the literature. Waves do not necessarily break up a monolayer on their own; however, the combination of wind and waves is believed to do this (Palada et al. 2012). Wind and decomposition factors are extensively mentioned in the literature.

Palada et al. (2012) indicated a lack of wind-wave modelling and experimental studies in the literature concerning impacts on monolayer performance. Understanding monolayer performance under wind-wave conditions will enable improved application of monolayers in real-world conditions. Experimental studies by Schouten, Palada, Lemckert, Sunartio & Solomon (2011) and Palada et al. (2012) and numerical simulations by Huang et al. (2011) using a spectral model all suggest that monolayer performance may occur at wind speeds lower than those generally observed in field. This seems reasonable for the Schouten et al. (2011) and Palada et al. (2012) studies as the fetch is limited. Evidently there is a mismatch between field observations and current laboratory trials. The spectral model used by Huang et al. (2011) suffers from a lack of individual wave resolution. The impact of wind-waves is indicative and is inferred from the significant wave height. The significant wave height is the average

of the highest one-third of wave heights in a wave record, or four times the standard deviation of the water surface about the mean still water level (Young 1999).

To complement these studies, CFD is proposed for modelling the average instantaneous shear stress under wave action to quantify the breakup of monolayers. Velocity gradients can be extracted from the flow domain and used to determine the instantaneous shear stress. Wind-waves are highly site specific and correlating shear stress to monolayer performance would require substantial investigation over a range of wind speeds and surface geometries. A preliminary model is presented in this dissertation.

1.2 Project Objectives and Scope

The aim of this work was to develop a CFD model to evaluate the average instantaneous shear stress produced under a range of wind speeds. The specific objectives of this research project were to:

1. Research wind-wave theory and the numerical modelling of wind-waves.
2. Research evaporation of water from reservoir bodies.
3. Research the effectiveness of monolayers in reducing evaporation under the action of wind-waves.
4. Develop a 2D / 3D Computational Fluid Dynamics (CFD) model for simulating wave generation by wind, incorporating two phases (air/water) in a representative reservoir.
5. Apply the developed CFD model to investigate water surface stretching in response to wave action under defined wind loading scenarios. Validate the model with numerical data from USQ, if available.
6. Critically analyse and discuss the surface stretching response and the implications of wind-waves on monolayer efficiency in reducing evaporation.
7. Investigate the scale-up applicability of the wind-wave results from model output to field trials.

8. Recommendations for further studies.

The CFD model is preliminary and it is a foundation upon which subsequent and more complex models may be built. Time permitting, the effects of reservoir bank slope on wind-wave heights was to be examined; this did not occur.

1.3 Methodology Summary

A review of literature was undertaken to determine the status of the numerical modelling of wind-waves affecting monolayer performance in reducing evaporation. This literature review confirmed the absence of numerical modelling of wind-waves in the context of monolayers, with the exception of the Huang et al. (2011) paper. This review provides a foundation on which to develop this project. ANSYS Fluent was used to develop a simple multiphase model of air over water. The model was based on an experimental wave tank used in the Schouten et al. (2011) and Palada et al. (2012) papers. Simulations were run for the constant velocity wind speeds 7.33 m/s, 4.11 m/s and 0.89 m/s, the limits being the observed monolayer performance range (Brink 2011). Sampling of velocity gradients and volume fractions was conducted. This flow field data was filtered using Microsoft Excel to identify shear stress near the water surface. The water surface values were not used due to limitations on the accuracy of velocity gradients at the interface. Matlab was used for the statistical analysis of the filtered data and plotting purposes. Statistical tests included the One-way Analysis of Variance test and the Kruskal-Wallis test on sample instantaneous shear stress. The effect of bank slope on wind-wave height was not addressed in this study.

1.4 Project Contributions

The contribution of this project to the literature is the development of a simple CFD model to examine the average instantaneous shear stress distribution of the water surface for a specific water basin under three wind loading scenarios. The shear stress provides a measure of the stretching of the water surface. Normal stresses were not

included as these do not cause shear deformation of a fluid. As monolayers are a surface film, this shearing stress can be used to infer the disruption of a monolayer film. Knowledge of monolayer disruption under wind-waves will assist in improving application of monolayers in storage reservoirs. This model is preliminary and it provides a foundation for further development. The reporting of average instantaneous shear stress against the limit wind speeds and recommendations for further studies indicates that the project objectives have been satisfied.

1.5 Consequential Effects

The consequential effects of this project may be briefly considered as: ethical, safety and sustainability issues. Ethically, this research project has been conducted in accordance with Engineers Australia principles identified in the Code of Ethics. There is no harm or loss to any individual person, group, or business. This research involves numerical simulations on a computer, consequently there are no safety implications beyond that of the author's general health in the conducting this project. The sustainability of water supply and agricultural industries is why this research is being undertaken and societal benefits are mostly positive. The only negative would like be a loss of recreational use of water reservoirs, as this would disrupt monolayers (McJannet et al. 2008).

1.6 Dissertation Outline

An overview of the chapters in this thesis is provided below.

1.6.1 Chapter 1. Introduction

Chapter 1 provides an overview of the use of monolayers for evaporation reduction in water reservoirs. Previous studies are introduced. The project aims and a summary methodology are provided. Project contributions are identified. A description of the remaining chapters in this dissertation is also presented.

1.6.2 Chapter 2. Background and Literature Review

Chapter 2 presents a review of relevant literature and selected background material covering the topics of evaporation, monolayers, wind-waves and computational fluid dynamics. The literature on numerical simulations of wind-waves affecting monolayers is limited to a few published articles. CFD modelling of wind-waves quantifying instantaneous shear stress at the water surface is not present in the literature.

1.6.3 Chapter 3. Methodology: Numerical Simulations

Chapter 3 presents the methodology used to investigate shear stress at the water surface. A preliminary wind-wave model is developed to determine the instantaneous shear stress at the water surface under three wind loading scenarios. Flow field velocity gradients and volume fractions were extracted. The distribution of shear stress is examined for steady-state conditions and statistics of mean, median and standard deviation are reported. ANSYS Fluent was used to develop a CFD model. Matlab 2010a was used for data analysis.

1.6.4 Chapter 4. Results and Discussion

Chapter 4 presents the results of the numerical simulations. Five samples were collected for each of the 7.33 m/s and 4.11 m/s wind speeds. Three samples were collected for the 0.89 m/s wind speed. The distribution of samples was examined. Data Analysis tests include One-way Analysis of Variance (ANOVA) and the Kruskal-Wallis tests.

1.6.5 Chapter 5. Conclusions and Recommendations

Chapter 5 highlights the main findings of the research, identifying the contributions of the project to the literature. A number of recommendations for further development of the preliminary model and for additional research on the broader subject of monolayer numerical simulation have been provided.

1.7 Summary

Chapter 1 has provided an introduction and overview of this dissertation. The project context, objectives and a summary methodology have been presented. An outline of the remaining chapters has also been presented.

Chapter 2

Background and Literature Review

Chapter 2 presents a review of relevant literature and background material for this dissertation. The review appraises the current state of knowledge concerning numerical simulation of monolayers under wind-wave action, specifically shear stress at the air/water interface, and highlights specific theoretical concepts. Surface stretching of the water is believed to break up the monolayer coverage under wind-wave action. This stretching, or instantaneous shear stress, is yet to be quantified in the literature. Knowing the shear stress corresponding to operational limits of monolayers, over a range of geometries , would permit estimates of monolayer performance for reservoirs.

The review of literature required accessing knowledge on a broad range of topics, including: evaporation, monolayers, wind-wave interactions, and computational fluid dynamics. A broad scope was necessary due to the complexity of the system being examined. Many questions had to be answered, including: What are monolayers? What factors influence their success in reducing evaporation? How do wind waves develop? How are wind waves described, both quantitatively and qualitatively? Have any wind wave studies concerning monolayers been completed? If so, what were the major findings? What numerical models, if any, have been applied? Understanding aspects of each of these topics was a challenge. The review of literature was extensive and the follow-

ing chapter presents only a snapshot of the literature reviewed over the course of this dissertation.

The literature review found that the factors influencing the success of a monolayer in reducing evaporation are numerous, and consequently the performance of monolayers are highly variable. Wind-waves are a major factor limiting monolayer success. Recent experimental studies suggest that monolayers may not be successful under field wind-wave conditions, in all but calm conditions. The review also found that only one computational study concerning monolayers under wind wave action is reported in the literature.

Chapter 2 is arrange thematically and covers the following topics in sequence: evaporation, monolayers, wind-wave studies, wind-wave theory, and computational fluid dynamics.

Evaporation loss from dams is a significant issue in Australia, where losses up to 40% of storage volume may be experienced (Helfer et al. 2011). CSIRO (2007) predict a reduction in rainfall intensity by up to 50% by 2070, depending upon location. Temperature is predicted to increase up to 5°C by 2070. For regional communities, agricultural and other water intensive industries, where water supply is from open reservoirs, a reduction in the stored water may present significant sustainability challenges. Many regional communities have had tight water restrictions in the previous decade, and this situation will likely remain. Consequently, reducing evaporation rates in storage dams is an important research focus.

Research centres with an interest in minimising evaporative losses in water storages include the National Centre for Engineering Agriculture (NCEA) based at the University of Southern Queensland (USQ) and the now defunct Cooperative Research Centre for Irrigation Futures (CRC). Research is also being undertaken at Griffith University (GU).

A number of evaporation mitigation techniques to reduce evaporative loss have been investigated in the last decade, with highly variable success being reported. Techniques include: wind breaks, destratification techniques, fixed covers and chemical monolayers.

Of these methods, fixed covers have been most successful, with reductions up to 91% reported when used (Helfer et al. 2011). Fixed covers provide a physical barrier which obstructs the movement of water molecules from the water body into the atmosphere. This easily explains why this method would be the most successful in reducing evaporation. Some success has been reported with wind breaks, whilst negligible results have been found with destratification technologies (Helfer et al. 2011). Destratification techniques focus on keeping the surface temperature cool through convection within water bodies. A limitation of fixed covers is that they are expensive to purchase and maintain for relatively large storages (Craig 2005). For large reservoirs, the use of chemical monolayers offers a cost effective alternative. Recent research efforts concerning reservoirs with a focus on monolayers include: the development of new monolayer products, the application systems, detection of monolayers on water body and wind-wave experimentation and modelling of monolayers (Schouten et al. 2011, Brink 2011, Coop et al. 2011, Huang et al. 2011, Palada et al. 2012).

Monolayers are artificially synthesised chemical films, one molecule thick, which spontaneously spread on contact with a water surface forming a effective surface barrier (Barnes 2008). Natural monolayers may also exist at the surface of a water body; however, the evaporation reduction potential of such monolayers is usually considered negligible, as they lack the surface pressure to reduce evaporation loss (Hancock, Pittaway & Symes 2011). Artificial monolayers are amphiphilic, having both a hydrophobic (water repellent) and hydrophilic (water attracting) component, which forces the monolayer to spread over the water surface. Figure 2.1 shows the amphiphilic nature of monolayers. Under favourable conditions, such monolayers have the potential to reduce evaporation rates up to 40% (McJannet et al. 2008). Traditional monolayers comprise stearyl alcohol (octadecanol) and cetyl alcohol (hexadecanol) products. In the last decade, the types of monolayers has been expanded to include prototype monolayers as investigated by Schouten et al. (2011). Such prototype monolayers are an attempt to overcome some of the performance issues with the octadecanol and hexadecanol type monolayers.

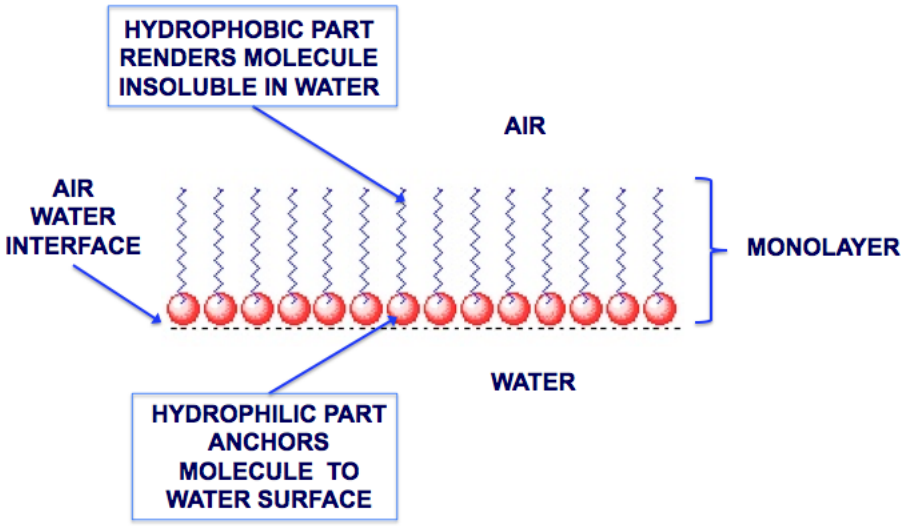

Figure 2.1: Amphiphilic nature of monolayers modified from Barnes (2008)

Wide variability in the performance of monolayer performance has been reported in field trials (Barnes 2008). A technical report by Hancock et al. (2011) indicates that the inconsistency in the observations is a consequence of the large number of inter-related environmental factors. This is understandable, natural systems can be highly complex. Factors affecting the performance of monolayers include: temperature of water, temperature of air, displacement by wind, wave field, relative humidity of air, ground seepage, presence of a natural monolayers, incident solar radiation, biological decomposition, surrounding terrain and the morphology of the dam. It is easily noticed that many of these factors are stochastic, varying temporally. Consequently, a deterministic solution for monolayer performance would not be easily determined. The complexity interrelated factors would suggest that predicting monolayer performance would be difficult. Of the number of factors influencing monolayer performance, wind and biological decomposition are generally considered to be the most detrimental and prevalent in the literature. Predictions of monolayer performance under winds are mostly qualitative (Palada et al. 2012). Under conditions with little to no wind, < 0.3 m/s the performance of monolayers is generally good, with 45% savings being achieved (Palada et al. 2012). 45% is quite a low reduction. Given that monolayers spread

spontaneously, it would make sense that the monolayer could be disturbed easily by wind-waves.

Significant detrimental effects on monolayer performance are the result of bacterial decomposition and break up due to wind-waves. These two factors are noticeably prominent in the literature. Bacterial decomposition restricts the life of an applied monolayer to approximately three days. For sustained evaporation resistance, a monolayer must consequently be reapplied every few days. Application rates and locations are important component of effective monolayer performance. Brink (2011) provides details on the development of a universal framework for monolayer application, which provides assistance in optimising monolayer application. Barnes (2008) states that almost all problems with monolayer performance stem from poor resistance under wind action. The action of wind both transports monolayer products across the water surface, and generating waves, which are believed to act to stretch and break the up the monolayer coverage (Schouten et al. 2011, Palada et al. 2012). As stated by Palada et al. (2012), a quantitative assessment of wind and wave impact on monolayer performance is yet to be substantiated in the literature. This is easily observed when reviewing the literature. The maximum wind speed for monolayers is reported as an average of 26.4 km/h (7.33 m/s) (Brink 2011).A t higher wind speeds, monolayers are considered ineffective. Wind induced drift of monolayers commences at approximately 3.2 km/h (0.89 m/s). Together these two limits comprise a generalised range over which monolayers have been observed to produce a reduction in evaporation, with decreasing evaporation resistance as wind speed increases. An understanding of wind-wave impact is necessary for monolayer performance prediction in a reservoir.

Quantitative experimental and computational studies of wind wave affects on monolayer performance are noticeably lacking in the literature. Palada et al. (2012) and Schouten et al. (2011) corroborate this observation. Observations are numerous and are summarised by McJannet et al. (2008) and Barnes (2008). The lack of experimental studies is understandable, as wind-wave experimental data is generally difficult and costly to obtain. This data acquisition difficulty is limited by sensor technology and the broad variability in atmospheric, water and wave fields (Sullivan & McWilliams 2010). The lack of numerical studies is also understandable, given the likely computational run

times required for the grid resolutions likely to be required. Quantitative experimental studies have been undertaken by Schouten et al. (2011) and Palada et al. (2012), and a numerical studies has been completed by Huang et al. (2011). A Computational Fluid Dynamics (CFD) study was undertaken by Craig et a (2006); however, wind-waves were not explicitly investigated here.

Quantitative experimental investigations of wind-wave effects on monolayer performance have been undertaken by Schouten et al. (2011) and Palada et al. (2012). These studies are briefly described before the limitations are presented. Both studies used a wave tank with a wind blower and a wave paddle. The Schouten et al. (2011) paper evaluated the performance of six prototype monolayers against octadecanol, whilst the Palada et al. (2012) paper only considered the octadecanol monolayer. Sinusoidal waves with a 6 second period and 2 centimetre height were used along with wind speeds between 0 and 5 m/s. The angle of incidence of the wind blower was varied for the Schouten et al. (2011) paper. Whilst these studies were of a very limited scope, both found that the octadeconal had poor evaporation resistance performance at wind speeds greater than 1.3 m/s. The prototype monolayers generally had a higher level of evaporation resistance. Both papers suggested that wind waves break up and stretch out a monolayer. Neither study included an examination of water surface shear stress in response to wind speed.

The scope of the Schouten et al. (2011) and Palada et al. (2012) papers was limited to several combinations of wind speeds and wave frequency. The wave amplitude was varied in the Schouten et al. (2011) paper through the varying the angle of incidence of the wind, which distorts the wave field. This is an attempt to produce wave field more representative of field conditions where an irregular confused surface evolved under a wind field. Wind waves may be considered an aggregation of many linear sinusoidal waves, aggregating in an irregular wave field. Many combinations on wind speed and wave amplitude would be necessary to evaluate the performance of monolayers, as stated by Palada et al. (2012). This would be correct. A possible alternative to varying the incidence angle, not considered in these studies, would be to vary the motion of the wave paddle. The wave paddle could vary the wave period and amplitude through use of random sampling from a known wave height probability density distribution. The

sampling would come from the distribution from a wave height time series for a specific reservoir of interest or a reservoir with similar environmental conditions and comparable size. In either case, the wind and waves need to be consistent with conditions that would be observed at a dam. Another limitation is the size of the experimental equipment. Actual dams allow waves to evolve over greater distances than can be replicated in an experimental tank. The tank is therefore fetch limited. Larger waves of lower frequency would seemingly have a less detrimental impact than high frequency waves. Overall, it appears to be difficult to replicate field observations of wind-waves in a laboratory. To complement such experimental studies, numerical simulations offer another means of evaluating wind-wave fields.

Limitations of the Schouten et al. (2011) study included the small number of wind-wave combinations tested and the short fetch. The Palada et al. (2012) study also has these limitations. Huang et al. (2011) attempted to address these limitations though the use of a numerical simulation using the spectral wave model on a full sized reservoir, Logan's Dam. Spectral models have been used for ocean wave forecasting by the Bureau of Meteorology in Australia for almost 20 years (BOM 2010). The spectral model uses a mean wind speed to evolve and transport the significant wave height (H_s). The significant wave height is the average of the highest one-third of waves in an observed wave field or four times the standard deviation of the surface elevation (Young 1999). Spectral models require significantly less computational time than phase resolving models, such as CFD, because they do not resolve individual waves. While phase resolving models are very sensitive to initial conditions, phase averaged models are not as individual waves are not resolved. Extensive effort has gone into refining the spectral model over the last 20 years and the theory is well developed (Janssen 2008). The Huang et al. (2011) study concluded that the spectral model could be used for indicative assessment of wave field development. Whilst the significant wave height was generally well modelled, the wave period was poor. A CFD study was undertaken by Craig, Mossad & Hancock (2006) to develop a model for predicting evaporation performance, however, wind waves were not investigated. No account of the water surface stretching was considered in this study. The development of an appropriate CFD model incorporating wind waves requires an understanding of how wind waves develop. Furthermore, the probability density function of wave heights would provide a

measure of the distortion of the wave surface; however, as shear stress includes velocity gradients it is arguably a better representation of surface distortion for estimating monolayer performance.

The study of wind waves has been extensive since the Second World War, when forecasting sea conditions for landing operations was desired (Janssen 2008). Wind waves is a challenging areas of study and progress has been hindered primarily due to difficulties with capturing experimental data under field conditions (Sullivan & McWilliams 2010). This is understandable considering the apparently complex feedback interactions between wind and waves. This limitation makes validation of wind wave models generally difficult. Despite this limitation, significant advances in wind wave theory has occurred, providing insight into how wind waves evolve and decay and facilitating the development of wind wave models, particularly the spectral model.

Field studies of the evolution of wind-waves provides insight into how an experimental and numerical simulation model should behave. Although wind wave evolution is complicated, the generally accepted process is described by Phillips (1957) and Miles (1957) theories, as cited in Young (1999), as follows: as wind blows over a calm water surface, pressure fluctuations over the surface give rise to small wavelets. As the wind speed increases, these wavelets receive additional energy from the wind and grow exponentially in height. As a wave field develops, there is shift from high frequency waves to lower frequency waves and from a narrow spectrum to a broad spectrum of wave heights and wavelength. Wave growth is limited by the fetch over which wind blows and the duration of wind blowing. The shift in frequency is due to nonlinear interactions between the waves (Janssen 2008, Mitsuyasu 2002). For enclosed basins, waves cannot propagate away from the generating area and so are reflected either partially or fully depending upon the basins edge geometry. The interactions would therefore be more complicated than in a wave field where the waves may travel out of the generating area under a wind. The extent to which reflected waves interact with a generating wave field would depend upon the size and aspect of the water surface. From this description, it is evident that wind waves in a water basin are a complicated phenomena. Statistical methods have been extensively used in the literature to quantify the wind wave field, and these have been successful at least for quantifying significant wave height.

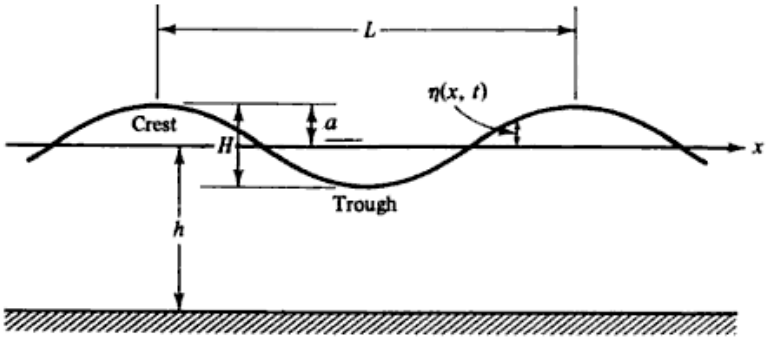

H

Figure 2.2: Wave Characteristics (Dean & Dalrymple 1991)

The evolution of a wave field is a complicated process. The observed chaotic water surface has been quantified using statistical methods. The variance of the surface elevation about the still water level, is equated to the energy of wave field (Young 1999). Through modelling the progress of energy using the spectral model, the wave field properties of significant wave height are determined under a given wind field. The spectral model assumes that waves are linear and comprises a number of finite sinusoidal waves of variable period and wavelength. Water waves are modelled reasonably well by linear theory (Young 1999). A simple linear wave is seen in Figure 2.2.

Equation 2.1 describes such a linear wave.

$$\eta = asin\left(kx - \omega t\right) = \frac{H}{2} sin\left(\frac{2\pi}{L}x - \frac{2\pi}{T}t\right) \tag{2.1}$$

Under linear theory, the wavelength is related to wave height through a dispersion relationship as shown in Equation 2.2 (Young 1999):

$$\omega^2 = \mathrm{g}k\tanh\left(kh\right) \tag{2.2}$$

For linear wave theory to apply, the waves must be considered deep. The wavelength relative to the water body depth must be less than 20 (Young 1999). For shallower dams, waves are affected by the presence of the dam floor and linear theory must be modified. Non-linear wave models account for slight raising of the wave crest and flattening of trough relative to still water level. Phase resolving models, such as CFD,

which are computationally intensive, are not required on ocean scales for forecasting purposes, only the general wave field conditions are approximated. Overall, the limitations on experimental data acquisition and the general wave field produced by a spectral model must be supplemented with phase resolved models, capturing the wave field for a better understanding of monolayer behaviour under wind-waves. CFD is a focus of wind-wave research to achieve this.

Computational fluid dynamics (CFD) involves the use of numerical algorithms to solve the governing equations of fluid mechanics and any transport equations for additional phenomena, for example, volume of fluid fraction. CFD studies of water waves are reported in the literature, including Bakhtyar et al. (2010), Wang et al. (2009),Lal & Elangovan (2008) and Lin et al. (2008) The governing equations include the conservation of mass, the conservation of momentum and the conservation of energy. Equations 2.3 to 2.5 are the two-dimensional governing equations for the conservation of mass and momentum in an x-y plane (Anderson Jr 1995).

$$\frac{\partial \rho}{\partial t} + \nabla \cdot (\rho \mathbf{V}) = 0 \tag{2.3}$$

$$\frac{\partial (\rho u)}{\partial t} + \nabla \cdot (\rho u \mathbf{V}) = -\frac{\partial p}{\partial x} + \frac{\partial \tau_{xx}}{\partial x} + \frac{\partial \tau_{yx}}{\partial y} + \rho f_x \tag{2.4}$$

$$\frac{\partial (\rho v)}{\partial t} + \nabla \cdot (\rho v \mathbf{V}) = -\frac{\partial p}{\partial y} + \frac{\partial \tau_{xy}}{\partial x} + \frac{\partial \tau_{yy}}{\partial y} \rho + f_y \tag{2.5}$$

The shear stresses are assumed to be equated to the velocity gradients as seen in equations 2.6 to 2.8:

$$\tau_{xx} = \lambda (\nabla \cdot \mathbf{V}) + 2\mu \frac{\partial u}{\partial x} \tag{2.6}$$

$$\tau_{yy} = \lambda (\nabla \cdot \mathbf{V}) + 2\mu \frac{\partial u}{\partial y} \tag{2.7}$$

$$\tau_{xy} = \tau_{yx} = \mu \left[\frac{\partial v}{\partial x} + \frac{\partial u}{\partial y} \right] \tag{2.8}$$

Solution to CFD problems involves the propagation of flow field variables in temporal and spatial domains (Tu et al. 2008). This propagation stems from an initial state. Boundary conditions result in a deterministic solution approximating a real flow field. For an identical model setup, boundary conditions and initial condition, CFD will generate the same solution. For turbulent flows, characterized by random fluctuations in flow field variables, solution of the governing equations is limited by the resolution of the mesh. Very fine scales are required to capture turbulent behaviour in the flow. Capturing such fine scales is limited by the computational power . As computational capabilities presently cannot resolves all scales for turbulence, the use of a Reynolds-averaged Navier-Stokes Equations (RANS), with an appropriate turbulent closure model is necessary (Tu et al. 2008). Large Eddy Simulation (LES) is an another alternative.

Present computational capabilities do not permit the governing equations of fluid mechanics to be solved over the full spectrum of turbulence scales for fully turbulent flows and high Reynolds Numbers, as stated by Tu et al. (2008). Such limitations mean that either the RANS equations are used with an appropriate turbulence closure model or an LES model are used. RANS models have one turbulence length scale, whereas LES models have some threshold below which the turbulence scales are not resolved. As LES models are computationally intensive than RANS, they are not considered further here. The RANS equations are derived from the momentum equation through use of a mean and fluctuating velocity components. Turbulent closure models are required to solve the additional stress terms produced by this approach. Different turbulence models are available and each is suited to particular cases. For this study only the two-equation $k - \varepsilon$ closure model is used. This model was shown by Bakhtyar et al. (2010) to give reasonable results over the computational domain in their investigation of waves breaking on a shore. Specifically, only where waves were not breaking was the model reasonable. Using the RANS equations with $k - \varepsilon$ model, the turbulent shear stress are related to the velocity gradient linearly seen in Equation 2.8. The instantaneous shear stress or stretching, of a fluid, is proportional to the shear strain rate for

a Newtonian fluid. This is what flow field parameter this study seeks to determine at the water surface. Equations 2.9 to 2.11 are the two-dimensional incompressible RANS equations discretized in an x-y plane (Tu et al. 2008). Incompressible flows have a constant density. Body forces have been neglected in these equations.

$$\frac{\partial \overline{u}}{\partial x} + \frac{\partial \overline{v}}{\partial y} = 0 \tag{2.9}$$

$$\frac{\partial \overline{u}}{\partial t} + \frac{\partial \left(\overline{u}\overline{u}\right)}{\partial x} + \frac{\partial \left(\overline{v}\overline{u}\right)}{\partial y} = -\frac{1}{\rho}\frac{\partial \overline{p}}{\partial x} + 2\frac{\partial}{\partial x}\left(\nu\frac{\partial \overline{u}}{\partial x}\right) + \frac{\partial}{\partial y}\left(\nu\frac{\partial \overline{u}}{\partial y}\right) + \frac{\partial}{\partial y}\left(\nu\frac{\partial \overline{v}}{\partial x}\right) - \left[\frac{\partial \left(\overline{u'u'}\right)}{\partial x} + \frac{\partial \left(\overline{u'v'}\right)}{\partial y}\right] \tag{2.10}$$

$$\frac{\partial \overline{v}}{\partial t} + \frac{\partial \left(\overline{u}\overline{v}\right)}{\partial x} + \frac{\partial \left(\overline{v}\overline{v}\right)}{\partial y} = -\frac{1}{\rho}\frac{\partial \overline{p}}{\partial y} + 2\frac{\partial}{\partial y}\left(\nu\frac{\partial \overline{v}}{\partial y}\right) + \frac{\partial}{\partial x}\left(\nu\frac{\partial \overline{v}}{\partial x}\right) + \frac{\partial}{\partial x}\left(\nu\frac{\partial \overline{u}}{\partial y}\right) - \left[\frac{\partial \left(\overline{u'v'}\right)}{\partial x} + \frac{\partial \left(\overline{v'v'}\right)}{\partial y}\right] \tag{2.11}$$

The additional Reynolds stress terms are approximated as shown in equations 2.12 to 2.14. A closure model is required to use these equations.

$$-\rho\overline{u'u'} = 2\mu_T\frac{\partial \overline{u}}{\partial x} - \frac{2}{3}\rho k \tag{2.12}$$

$$-\rho\overline{v'v'} = 2\mu_T\frac{\partial \overline{v}}{\partial y} - \frac{2}{3}\rho k \tag{2.13}$$

$$-\rho\overline{u'v'} = \mu_T\left(\frac{\partial \overline{v}}{\partial x} + \frac{\partial \overline{u}}{\partial y}\right) \tag{2.14}$$

Shear stress is proportional to the velocity gradients in a Newtonian fluid. Knowing the velocity gradients, the instantaneous shear stress can be determined. Shear stress is highest in the boundary layers of a fluid, either where fluid is in contact with a wall or at the interface with another fluid of significantly different viscosity. As shear stress measurements at the water interface would be difficult to obtain experimentally, CFD is used here to investigate these. Velocity gradients can be extracted near the air/water

interface for an appropriately discretized grid and the instantaneous shear stress at the interface is determined. Locating the interface requires either interface-tracking or interface-capturing methods.

Determining the instantaneous shear stress at the water surface requires knowing the location of the water surface. Methods available to locate the water surface are either interface-tracking or interface-capturing. Interface-tracking methods require deformation of the mesh to follow the interface. Interface-capturing methods move the interface through a fixed computation domain, with the interface being located in cells that are partially filled with water and air fractions. Interface-tracking methods are more accurate; however, additional computational power is required and complex geometries are limited when compared with interface-capturing methods. Interface-capturing method have less accuracy with location of surface (Gerlach et al. 2006). Two common interface tracking methods are Volume of Fluid (VOF) and level-set approaches. Gerlach et al. (2006) and ANSYS (2011) compares these methods. For this study, the common VOF approach will be used. The VOF method is limited in accuracy near the air water interface because the spatial gradients of volume fraction are not continuous across cells. This would suggest that only cells with either water or air fractions should be used when examining velocity gradients to determine the shear stress.

The Volume of Fluid method requires transport of a scalar quantity F, the volume fraction of a cell through the computational domain. Figure 2.3 shows the volume fraction of water in computational cells.

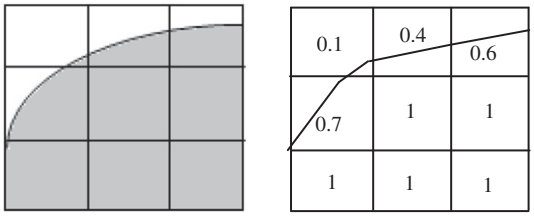

Figure 2.3: Volume of Fluid Method (Bakhtyar et al. 2010)

The governing equations of mass and momentum are solved with a conservation equation for the volume fraction, Equation 2.15 and density and dynamic viscosity values

computed from Equations 2.16 and 2.17 (Gerlach et al. 2006).

$$\frac{\partial F}{\partial t} + \nabla \cdot (\mathbf{V}F) = 0 \tag{2.15}$$

$$\rho(F) = \rho_w F + \rho_a (1 - F) \tag{2.16}$$

$$\mu(F) = \mu_w F + \mu_a (1 - F) \tag{2.17}$$

Commercial and Open-Source software is available for CFD simulations, including the Volume of Fluid approach to interface-capturing.

Commercial and open-source software is available for CFD studies. Of the software available, only ANSYS Fluent and OpenFOAM were considered for this study. Access to both software was available. ANSYS had a graphical user interface (GUI), extensive supporting documentation and noticeable prominence in the literature reviewed. OpenFOAM lacks a user interface and extensive documentation. A GUI and extensive supporting documentation were the primary reasons for choosing ANSYS Fluent to undertake CFD studies.

In chapter 2, a literature review has been undertaken, addressing the numerical simulation of monolayers under the action of wind waves. Specifically, the topic of shear stress or surface stretching at the air water interface was reviewed. Surface stretching of the water is believed to break up the monolayer coverage under wind wave action. Limited experimental and numerical studies were found. These studies highlighted that wind-wave action was a significant detriment to the performance of monolayers in reducing evaporation rates. A single numerical simulation using a spectral model was found to offer indicative wind-wave sizing for a water storage dam. No CFD studies with a specific focus on wind waves water shear stresses and monolayers were found. Using the Volume of Fluid approach, this dissertation will complement the literature in providing additional insight into how surface stretching under generally accepted wind load limits can be used to infer monolayer performance.

Chapter 3

Methodology: Numerical Simulations

Chapter 3 presents the methodology for undertaking a numerical simulation of a simple reservoir to determine the average instantaneous shear stress at the water surface under generally observed monolayer performance wind limits. Shear stress has not previously been quantified in the literature regarding monolayer performance. It is suspected that monolayers break up under the action of waves and wind. The evaporation resistance of monolayers is reduced under such action. Knowledge of the average shear stress at the observed operational limits of monolayers, for a range of surface geometries, will permit estimation of monolayer performance in reservoirs provided the water surface shear stresses under wind loading are known. The simple model in this project is one of many possible geometries.

CFD is the method of choice for this study, as experimental measurement of velocity gradients across large dams would be difficult and cost prohibitive. The purpose of CFD is to provide insight into areas where experimentation is not easily undertaken or the work is cost prohibitive. The distribution of water surface instantaneous shear stresses under wind loading is one such scenario. The validation of such numerical models is subsequently difficult. For a particular reservoir, should the shear stress of the water surface be quantified, then the performance of a monolayer may possibly be

inferred at other reservoirs. The results are specific for the geometry modelled and subject to a number of limitations and assumptions.

Chapter 3 reviews what flow field data was collected, how the data was collected using the software ANSYS Fluent, how the flow field data was analysed to produce average instantaneous shear stress, and provides comments on validation of the numerical model.

3.1 Flow Field Data

This section describes what flow field data was collected and where it was collected.

Flow field data was collected at each node within the two-dimensional structured computational domain with a square mesh. Table 3.1 lists the flow field data extracted from the ANSYS Fluent model.

Table 3.1: Flow variables collected

Node Coordinates (m)	Velocity (m/s)	Velocity Gradients (1/s)	Volume Fraction
X-coordinate	Velocity magnitude	Strain rate magnitude	Phase 1 (air)
Y-coordinate	$\mathbf{V}_x$	$\partial \mathbf{V}_x / \partial x$	Phase 2 (water)
	$\mathbf{V}_y$	$\partial \mathbf{V}_y / \partial x$	
		$\partial \mathbf{V}_x / \partial y$	
		$\partial \mathbf{V}_y / \partial y$	

The variables listed in Table 3.1 were collected for the following reasons: Node coordinates identify the corners of the control volume cells in the computational domain. All flow field variables extracted from nodes are the average of the surrounding cell-centre values. Flow velocity was extracted at each node, this was not used in analysis, but rather was to provide a general check of velocity profiles in the domain. The strain rate magnitude includes contributions from the normal strain rates, $\partial \mathbf{V}_y / \partial y$ and $\partial \mathbf{V}_x / \partial x$. It is incorrect to use the strain rate as the normal velocity gradients are not used for

determining shear stress. The shear stress or stretching rate of a fluid is proportional to the velocity gradients, $\partial \mathbf{V}_y/\partial x$ and $\partial \mathbf{V}_y/\partial x$, for a Newtonian fluid. The extraction of these velocity gradients is necessary to determine rate of shear strain and subsequently the instantaneous shear stress. The volume fractions allow identification of the interface within the computational domain. Cells with a volume fraction other than 1 or 0 contain an interface.

Data was collected at sample nodes within the computational domain. Figure 3.1 shows the sampling region relative to the computational domain.

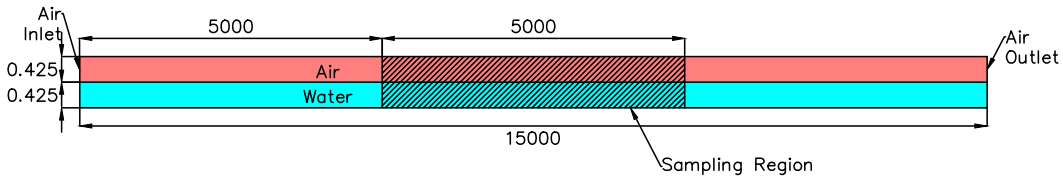

Figure 3.1: Computational Domain and Sampling Region

The sampling region from 5 to 10 m, was chosen to be 5 m away from the inlet and the outlet of the tank to minimise the effects of the inlet and outlet boundary conditions on the sampling region. Inspection of the phase and horizontal velocity gradient profiles, seen in Appendix B, shows that this sampling region is acceptable and free from the influence of the inlet and outlet boundary conditions. Waves are propagating in the sampling region alone. Furthermore, the immediate effect of the presence end walls on flow velocity is removed.

Flow field data was collected for three wind speeds U_{inlet}: 0.89 m/s, 4.11 m/s and 7.33 m/s, at intervals slightly larger than the residence times for each wind speed. These lower and upper wind speed correspond with the observed limits for monolayer performance (Brink 2011). Residence time is defined as the time for an air parcel to travel from the inlet of the tank to the outlet of the tank. Residence time was calculated using Equation 3.1, which is a simplification of the three-dimensional case of volume

divided by flow rate.

$$t_{res} = L_{tank}/U_{inlet} \tag{3.1}$$

The residence time intervals and sample times are summarised in Table 3.2.

Table 3.2: Summary of wind speed sampling times

Wind Speed (m/s)	No. Samples	Residence Time (s)	Sample Times (s)
7.33	4	2.05	2.05, 4.10, 6.15, 8.20, 10.6
4.11	5	3.65	3.65, 7.31, 11.0, 14.6, 18.8
0.89	2	16.9	17.0, 34.0, 51.0

Residence time intervals for sampling were used to ensure that the data samples were independent of each other. Specifically, one sample was collected per parcel of air travelling from the inlet to the outlet over the duration of each consecutive residence time. Strictly, the fluid flow samples for the water will not be independent of each other. Waves generated over one sampling period will influence the next sampling period due to reflection of waves from the rear tank wall and because waves are propagating slower than air. The number of samples extracted is limited by the computational run time. For the slower wind speeds, the residence time is substantially greater than at higher wind speeds. The instrument for collecting the flow field data is ANSYS Fluent and it is described in Section 3.2.

3.2 Instrument: Software ANSYS Fluent

This section describes the use of the Computational Fluid Dynamics Software ANSYS Fluent workbench to extract the flow field data as specified in Section 3.1 of this Chapter. Pre-processing, solving and post-processing stages are presented.

Flow field data was collected using the CFD software ANSYS Fluent Workbench. This software was accessed online through the Remote Access Laboratory (RAL) at the

University of Southern Queensland (USQ). ANSYS Fluent was selected in preference to OpenFOAM due to the availability of GUI, extensive documentation and prominence of this software in the literature. Having completed this dissertation using ANSYS Fluent, it is now easier to understand how OpenFOAM could be used without a GUI.

Pre-processing involves defining the computational domain, subdividing the domain into appropriate control volumes, assigning fluid properties and specifying boundary conditions.

As seen in Figure 3.1, the two-dimensional computational domain is a 15 m long x 0.85 m high rectangle, divided into two zones of air and water, both 0.425 m high. Air is located above the water. The domain was based on the experimental tank used in a studies by Schouten et al. (2011) and Palada et al. (2012) with simplified boundary conditions for the inlet and the outlet.

The simple geometry of the computational domain permits a structured square mesh is used in preference to a unstructured mesh. This simplifies referencing of nodes and makes post-processing of data simpler. The air and water zones were subdivided into a relatively coarse 0.025 m square mesh. As this study is only a preliminary investigation, a grid independence study was not undertaken. Further refinement to the mesh size would have increased the computational run time, which was a constraint for this study. A grid independence study is necessary though to ensure that the flow field variables are not unduly influenced by the mesh resolution; a coarse grid is not likely to yield sufficient accuracy. Furthermore, mesh refinement near the interface and boundaries was not undertaken. The mesh should be refined to properly capture the velocity gradients in the vicinity of all interfaces.

The fluid properties used in this study were the default values for air and water available in Fluent. Water default values of density and dynamic viscosity were: 998.2 $kg.m^{-3}$ and 0.001003 $kg.m^{-1}s^{-1}$. Air default values of density and dynamic viscosity were: 1.225 $kg.m^{-3}$ and 1.7894E-5 $kg.m^{-1}s^{-1}$. The volume of fluid method relies on fluids being immiscible and there is no change to the relative humidity of the air and it is unsaturated here. In a real reservoir, density and viscosity would vary as the temperature of the fluids change. Pressure variations would modify the density as well. A

monolayer was not included in the model. Being one molecule thick, the grid resolution is not fine enough to permit inclusion. Modelling may be possible should a microscopic level be examined.

Boundary conditions are necessary to solve the governing equations of fluid dynamics for a specified computational domain. These conditions define how a real fluid behaves at all boundaries of the domain. Boundaries conditions are specified at the inlet and outlet regions, all walls and the interfaces between water and air. Figure 3.2 shows the boundary conditions used in this study.

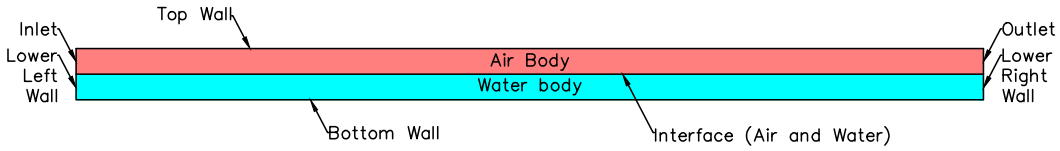

Figure 3.2: Named Boundary Conditions

Table 3.3 presents summarises the boundary conditions used in this study.

Table 3.3: Flow variables collected

Boundary Name (m)	Condition Specified
Walls	Wall. No slip.
Inlet	Velocity inlet. Constant uniform.
Outlet	Pressure outlet.
Interface	Interface.
Interior	Interior.

No interaction was specified at the air/water interface; hence, no surface tension. Furthermore, a mesh interface was created between the air and water. The inlet velocity profile generated waves where the inlet contacted the water surface. Waves are also generated at the outlet due to the pressure reduction; a consequence of the model setup.

The solving stage involves specifying the flow models, initial conditions, spatial and temporal solvers, convergence criteria, time step and iteration parameters and the running of computations.

The Volume of Fluid and standard $k-\varepsilon$ models were specified. The Volume of Fluid model has two phases: air and water. The implicit body force option was specified. The standard $k-\varepsilon$ turbulence closure model was specified with default model constants. It was chosen as it has less equations to solve that other more complex turbulence models and therefore less computational runtime. The key considerations here were reduced runtime and adequacy of the model. The Reynolds stress turbulence closure model is considered to be better for modeling swirls and rapid strain rate changes (ANSYS 2011); however, as significant swirls are not expected in the flow, the $k-\varepsilon$ model was considered acceptable for preliminary studies. The $k-\varepsilon$ model was shown by Bakhtyar et al. (2010) to give reasonable results over the computational domain in their investigation of waves breaking on a shore, specifically where waves were not breaking. The $k-\varepsilon$ models assumes the flow is fully turbulent, as it should be for most wind fields. Furthermore, the solution is transient, not steady state. Double-precision was used.

Initial conditions for the transient solution were specified as follows: The water zone was patched with volume fraction of one. Gauge pressure of zero was applied. Initial velocity conditions throughout the domain were zero. Both the Turbulent Kinetic Energy (TKE) and Turbulent Dissipation Rate were left as defaults of 1 $m^2.s^{-2}$ and 1 $m^2.s^{-3}$ respectively. The TKE and dissipation rates should be varied; however, this requires further investigation.

Solution methods were specified as follows: The Pressure-Velocity Coupling was PISO with skewness and neighbour correction values of one. Spatial discretization involved: Least Squares Cell Based Gradient, PRESTO! Pressure, Second Order Upwind Momentum, TKE and Turbulent Dissipation Rate, Geo-Reconstruct Volume Fraction. First Order Implicit Transient Formulation was used, as second order was not permissible.

Convergence criteria were specified as follows: All convergence residuals for convergence were set at 10E-7. A small residual is necessary for accuracy.

Time step and iterations were specified as follows: For the 7.33 m/s and 4.11 m/s runs, the time steps were set to 20 iterations with variable time stepping, commencing at 1E-6. For the 0.89 m/s runs which required a long run time to reach residence time multiples, fixed time stepping of 0.0001 was used with 10 iterations per run. The global courant number was specified as 1. Variable time stepping was initially used for the 0.89 m/s run before switching to fixed time stepping and restarting the computations. The variable time stepping was used here to identify what time step size would be appropriate; 0.0005 was chosen. Non-iterative time advancement (NITA) was investigated to speed up the solution, however, this approach was abandoned as the residuals escalated relatively quickly into the low accuracy range. This was not observed when NITA was not specified.

Post-processing involves the manipulation of flow field data files exported during the solving stage. Solution data was exported at 34,000 time steps for the 0.89 m/s run. The 7.33 m/s and 4.11 m/s runs, with variable time stepping, were stopped manually and solution data was exported. This data is manipulated using Microsoft Excel for Mac 2011 (MSExcel) and Matlab R2010a as described in Section 3.3. Originally, all analysis work was planned to be completed in MSExcel; however, it was quickly realised that MSExcel was very inefficient when handling the large data files. No graphs were exported from ANSYS Fluent, rather phase and velocity gradient plots were constructed from the exported data using Matlab. These plots specifically focusing on the domain of interest, 5-10 m along the tank from the inlet. The exported domain extended from -15 m at the inlet to 0 m at the outlet horizontally, and 0 to 0.85 m vertically.

Problems with the data collection method included: remote access to the ANSYS Fluent software and the explicit solver scheme for the Volume of Fluid method. Remote access issues included: limitations on the number of booking sessions available for simulation runs, double-booking of sessions, remote access dropping at the university end, and the small storage space available for the noticeably large ANSYS Fluent project files. Considerable effort was put into resolving these issues; however, the collection of sample data was hindered. These matters were not originally anticipated to be a problem. Alternative access to ANSYS was unable to be arranged. The use of the explicit solver for the Volume of Fluid method is believed to be the reason why small time steps were

required for the 0.89 m/s run. It was expected that a time step greater than those used in the 7.33 m/s and 4.11 m/s samples could be used. Furthermore, with a reduction of iterations from 20 to 10 per time step, the 0.89 m/s solution data is likely to be less accurate than the high wind speed runs. Despite these issues, sample flow field data was successfully collected. Section 3.3 describes the analysis of this data.

3.3 Flow Field Data Analysis

Section 3 covers the post-processing of the flow field data exported from the ANSYS Fluent models. The general procedure for data analysis is as follows: the data was generally filtered to produce samples covering the specific subdomain located 5 to 10 m from the inlet. A specific filter was then used to extract flow field near water surface horizontal and vertical velocity gradients. These velocity gradients were then converted into instantaneous shear stresses. A relative frequency distribution of each sample was examined. Sample mean, median and standard deviations for each sample were subsequently plotted. A one-way analysis of Variance (ANOVA) test and Kruskal-Wallis test were used to examine whether the difference in instantaneous shear stress means and medians were significant to a 0.05 level. Lack of significant difference suggests that the samples are derived form the same population distribution. Samples from the same population may be aggregated. Samples were aggregated where non-significant mean differences were present and then plotted against wind speed. Details regarding the analysis procedure are now presented.

Flow field data, as listed in Table 3.1, was exported from ANSYS Fluent covering the entire computational domain. The format was ASCII with headings as follows: x-coordinate, y-coordinate, velocity-magnitude, x-velocity, y-velocity, strain-rate-mag, dx-velocity-dx, dy-velocity-dx, dx-velocity-dy, dy-velocity-dy, phase-1-vof, phase-2-vof.

General filtering was completed in MSExcel. Here, all data in the horizontal regions from 0 m to <5 m and >10 to 15 m was removed. Only the middle third of the tank was used for analysis. Once general filtering was completed, selected data was then imported into Matlab for the generation of phase plots and horizontal velocity gradient

plots. The Matlab contourf function was used for plotting purposes. See Appendix F.0.16 and F.017 for Matlab plotting scripts of phase and horizontal velocity gradient. Phase plots provide a qualitative view of the wave disturbance at the interface.

Specific filtering was also completed using MSExcel. This approach proved to be very inefficient. The middle third of the tank, from 5 to 10 m inclusive comprised 201 nodes horizontally and 36 data nodes vertically. The interface node was exported twice, as there were two boundaries at the air/water interface. Lines 18 and 19 of each vertical section were identical.

The shear stress at the water interface was required and this was no easy matter to obtain. Three specific filtering options were considered, with only one being reasonable for the available data. The first two options were not used as they were for cell-centred data. The third and selected option was for node values representing the average value of the surrounding nodes. This corresponds with the solution data exported. Cell-centred values should have been exported. Inspection of the flow field data shows that the velocity gradients in the water phase are substantially smaller than the air phase, as expected. Options two and three were proposed by the author in response to option one being inadequate.

The first option was to use a weighting function on the cell-centred nodes which have a volume fraction in them. There should be a single node with a volume fraction for each x-coordinate along the computational domain. The weighting function would sum the volume fraction of air and water, multiplied by their respective dynamic viscosities. This weighting function would be multiplied by the sum of the horizontal and vertical velocity gradients as per Equation 2.8 to determine the shear stress. This option was not considered acceptable as velocity gradients are limited in accuracy due to discontinuities in the volume fraction across cells with volume fractions other than zero or one.

The second option was to use the cell-centred node values closest to the air/water interface for which the volume fraction of water was one. The reasoning here is that should the grid be fine enough, then the cells will be located close enough to the interface to provide a reasonable estimate of the velocity gradients and consequently the shear stress. This also removes the volume fraction discontinuity concern.

The third and selected option is similar to option two, except that it works on the node-averaged locations, not cell-centred locations. At a given x-coordinate, the node closest to the interface with a volume fraction of one is used as the representative water surface node. Velocity gradients are extracted here. Figure 3.3 shows option two and option three. Clearly, the cell-centred option is closer to the interface than the node-averaged option; however for a sufficiently fine mesh, the difference should be negligible.

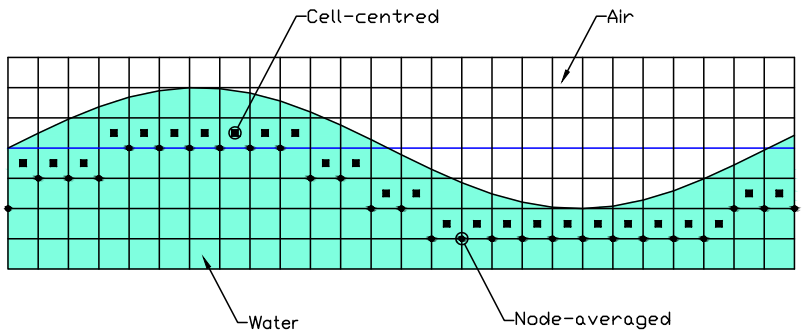

Figure 3.3: Specific sampling points, node-averaged vs cell-centred

Having identified the appropriate nodes to extract velocity gradients from, these were extracted for each x-coordinate between 5 m and 10 m inclusive using MSExcel. The shear stress was subsequently determined at these points by summing the horizontal and vertical velocity gradients and multiplying the sum by the dynamic viscosity of water. This method produced 201 shear stress values for each sample time, under each wind speed, which comprise the complete data set for further analysis in Matlab.

Relative frequency plots provide a qualitative overview of the spread of shear stress values within a sample and their centring. The shape of the distribution and any noticeable outliers can be inspected. Matlab scripts were written to plot the relative frequency distributions. A sample script is shown in Appendix F.0.18. Imported shear stress samples were divided into 20 bins each and the frequency of observations within the limits of each bin were counted. Too few bins smooth the data unnecessarily, too many bins under smooth the data. To complement the distribution plots, shear stress profile plots were produced. These plots show the shear stress value for each specifically x-coordinate node in the sample domain. Appendix F.0.19 shows the Matlab script for

these plots.

Having examined the relative frequency, sample statistics were subsequently examined through plotting, specifically, the mean, median and standard deviation. Appendix F.0.20 provides a sample script written for this purpose. The sample times in these statistics were normailsed by the residence time. Normalising allows direct comparison of the shear stress between different wind speeds. Having plots of the statistics, it is then necessary to determine which samples, if any, are not statistically significant, such that samples may be aggregated and the resultant average shear stress determined.

A One-way Analysis of Variance (ANOVA) test was used to determine whether any sample means, for a given wind speed, were likely to be from the same parent distribution. The ANOVA test returns a probability value under the assumption that all samples are drawn from populations with the same mean. A probability near zero suggests that at least one sample is significantly different to the other samples. The adopted significance level was 0.05. Similarly, a Kruskal-Wallis (KW) test was used to compare the sample medians. For data with outliers, the median provides a better measure of the sample centre, as the mean is sensitive to outliers. Matlab was used to complete the ANOVA and KW tests. Following these tests, the multicompare function was used to complete a pairwise comparison between samples determining which samples have means or medians statistically significant from other samples for a given wind speed. Appendix F.0.21 and F.0.22 indicate the Matlab scripts written to undertake the ANOVA, KW and multiple comparison tests.

Finally, for each wind speed, following the multiple comparison test of means, the highest sample means which are not statistically significant from those below were aggregated to determine an average instantaneous shear stress. Appendix F.0.23 presents a Matlab script written to plot these aggregated values against wind speed.

3.4 Model Validation

Validation is necessary when undertaking any numerical modeling. Validation is usually in the form of comparative tests between observed experimental results and the output

of a numerical model. If the model output is considered reasonable, then it may be appropriate for use. No experimental data is available for validation of the shear stress at the water surface, as determined in this study. Such data acquisition would likely be costly and difficult to acquire. It would be possible to compare observed wave height distributions from a real dam with those of a numerical model; however, owing to the multitude of factors influencing the model output, it is unlikely that wave height alone could be used to justify the accuracy shear stresses reported. This is a preliminary study, an investigation into validation options would need to be completed with further research. Velocity gradients may also be determined from particle image velocimetry (PIV) (Veron, Saxena & Misra 2007).

3.5 Importance and Limitations

There are a number of limitations in the methodology presented in this chapter, these limitations will be presented in the Results and Discussion chapter. The results provided by this study provide a foundation for further studies to undertake more detailed numerical simulations using CFD to assist with the evaluation of monolayer success in reservoirs under wind-wave action.

3.6 Summary

Chapter 3 has presented the methodology used to undertake numerical simulation of water waves in a tank. The focus was determining shear stress at the water surface. Three wind speeds were applied to a simple air/water domain, the limits being the generally accepted monolayer performance thresholds. Surface gradients were extracted using a specific filter method. Analysis was completed using both Matlab and MSExcel to produce a shear stress vs wind speed plot. Validation was briefly discussed. Chapter 4 presents the results of applying this methodology and discussed the implications and limitations of the results. This average instantaneous shear stress complements the existing literature, which is deficient in monolayer performance under break up caused by wind waves.

Chapter 4

Results and Discussion

Chapter 4 presents the results of applying the methodology of Chapter 3 and presents a critical discussion of these results. This chapter is organised around the following themes: general statements of results, comparison with previous studies, expected and unexpected results, and the remaining work, limitations and possible future work to be completed.

4.1 General Statements of Results

Key results are presented in this section. The order of results reflects the methodology presented in Chapter 3.

4.1.1 CFD Phase and Horizontal Velocity Plots

Figures 4.1, 4.2 and 4.3 show the volume fraction of air plots for wind speeds 7.33 m/s. 4.11 m/s and 0.89 m/s. Waves were seen to occur only at the air/water interface and were observed at all three wind speeds. The wavelengths appear shorter and wave frequency is higher at the 7.33 m/s wind speed. The wave magnitude is larger at 7.33 m than 0.89 m/s. Long wavelength waves progress from the inlet side of the sampling region. Shorter wavelength waves progress from the outlet side of the sampling region.

Larger and more frequent disturbances at higher wind speeds would disrupt monolayer coverage more significantly than the waves at lower wind speeds. Phase plots for all samples in the sampling region of the computational domain are shown in Appendix B.

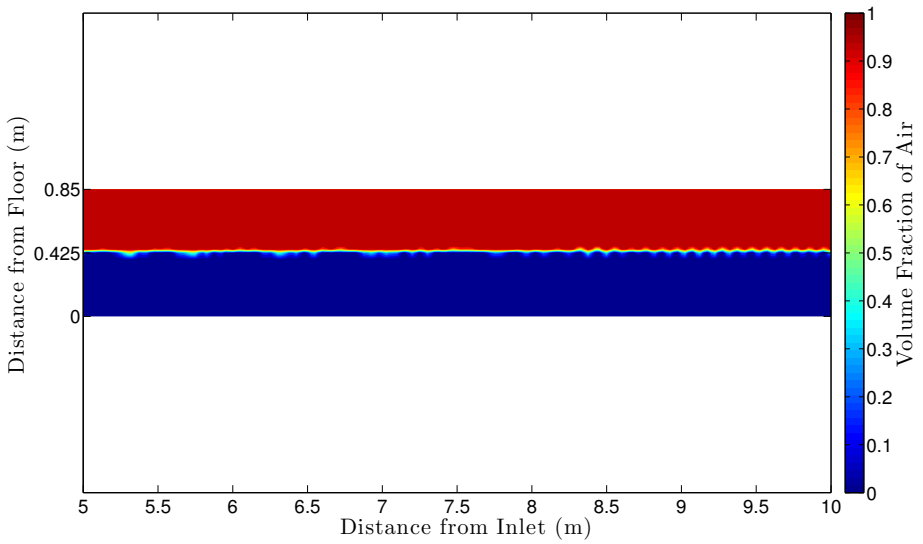

Figure 4.1: Wind Speed 7.33 m/s, Phase Plot, 10.6 s

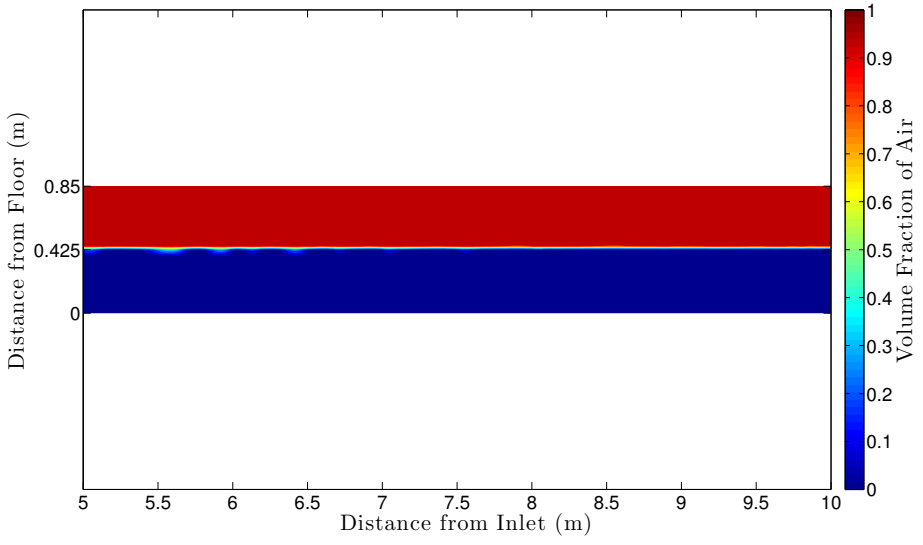

Figure 4.2: Wind Speed 4.11 m/s, Phase Plot, 18.8 s

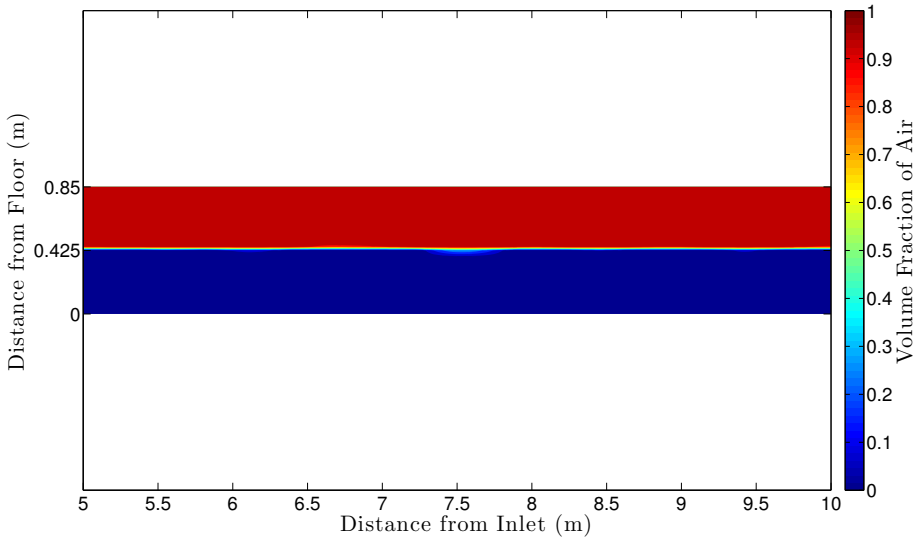

Figure 4.3: Wind Speed 0.89 m/s, Phase Plot, 51.0 s

Figure 4.4 shows a plot of the horizontal velocity gradient for the 7.33 m/s wind speed at 10.6 s. Horizontal velocity gradient is seen to be highest just above the air/water interface and at the roof of the tank, as expected. The velocity gradient drops quickly above the interface at the water level reflecting the significant change in density of the fluids when moving from air to water. The variation in the water horizontal velocity gradient in the water is substantially less than in the air phase and is not resolved in the plot. The velocity gradient behaviour is as expected. Horizontal velocity gradient plots for all samples in the sampling region are shown in Appendix B.

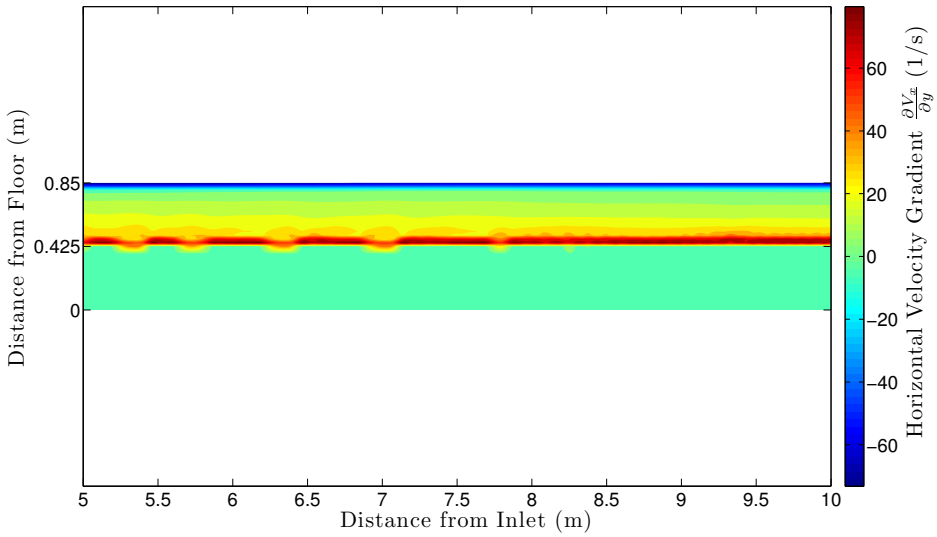

Figure 4.4: Wind Speed 7.33 m/s, Horizontal Velocity Gradient Plot, 10.6 s

4.1.2 Instantaneous Shear Stress Time plots

Figure 4.5 shows the profile of the sampled instantaneous shear stresses used to approximate the water surface shear stress. These instantaneous shear stresses were extracted using the specific filtering method outlined in the methodology. The shear stresses observed on the inlet side of the sampling region are larger than the stresses on the outlet side. This is consistent with the larger wavelength waves being observed on the inlet side previously in the phase plots. Shear stress is observed to generally increase with wind speed as expected. Shear stress profiles for all samples in the sampling region are shown in Appendix C.

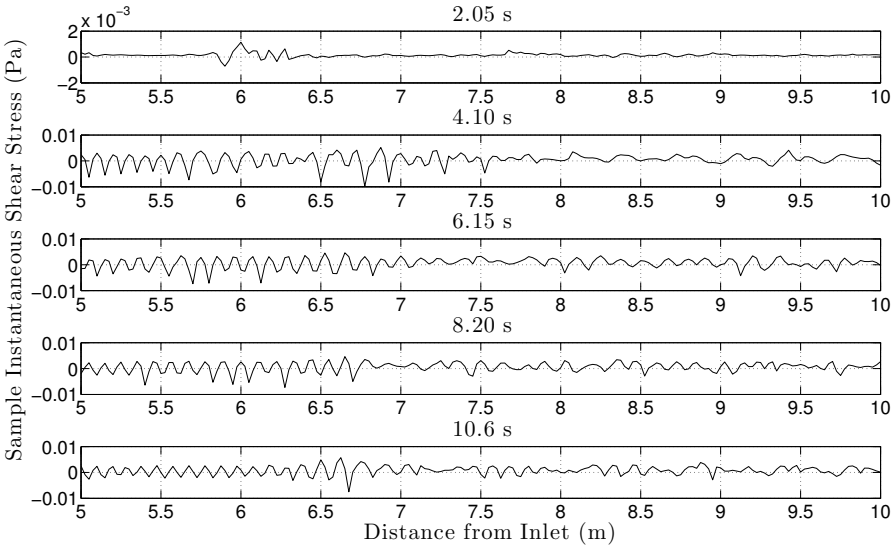

Figure 4.5: Shear stress time profiles, wind speed 7.33 m/s

4.1.3 Relative Frequency Distribution

Figure 4.6 shows the shear stress relative frequency plots for the 7.33 m/s wind speed at sample times between 2.05 s through to 8.20 s inclusive. The general behaviour observed for all wind speeds is a downshift from a relatively narrow high peak distribution close to zero to a broad lower peak distribution away extending away from zero. This broadening reflects an increase in the range of the instantaneous shear stresses sampled. With the exception of the first sample time for each wind speed, the distributions appear to have a approximately skewed normal distribution shape. The skew being evidence of waves progressing into the sampling region of the computational domain. The skew is primarily negative for the 0.89 m/s wind speed reflecting a wave propagating from the outlet side. The skew is less pronounced in the 4.11 m/s and 7.33 m/s wind speeds where waves travelled in both directions. The initial sample appears to have an approximate students t-distribution, reflecting the heavy tails on an otherwise normal distribution. The skewed normal and students t-distribution are only speculative and based upon visual inspection. Actual fitting of distribution functions has not been carried out as it is not critical for a preliminary model. An approximately normal distribution is necessary for using the one-way ANOVA test, along with a relatively similar variance.

Distribution plots for all samples in the sampling region are shown in Appendix D.

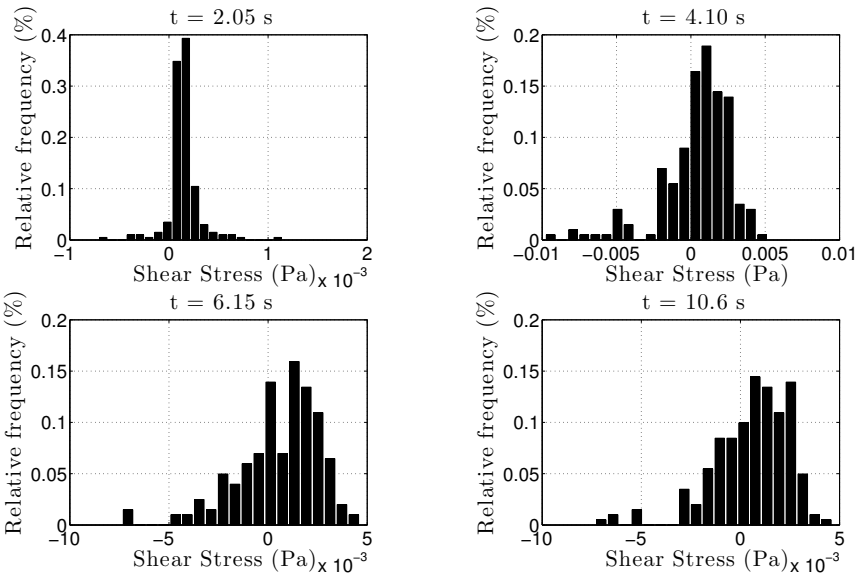

Figure 4.6: Shear stress time distributions, wind speed 7.33 m/s

4.1.4 Samples: Mean, Median and Standard Deviation

Figure 4.7 shows the sample average shear stresses against normalised sampling time. The instantaneous shear stresses increases with a larger magnitude wind speed. The 7.33 m/s wind speed develops larger shear stresses at a faster rate than the 4.11 m/s. The presence of a wave travelling from the outlet side is reflected in the negative trend of the 0.89 m/s sample averages with time.

Figure 4.8 shows the sample median shear stresses against normalised sampling time. Here there is a definite increase in the shear stress with time for all samples. Again, the 7.33 m/s develops higher shear stresses at a faster rate than the 4.11 m/s sample. When compared with the mean plot, the negative skew has been removed. This is expected as the median is not sensitive to high values.

Figure 4.9 shows the sample standard deviation shear stresses against normalised sampling time. All samples have an initial increase in the standard deviation, at least initially. For the 7.33 m/s sample, the initial increase is followed by a gradual reduction. The 4.11 m/s sample appears to be flattening with increase sample time. The

0.89 m/s sample is only increasing.

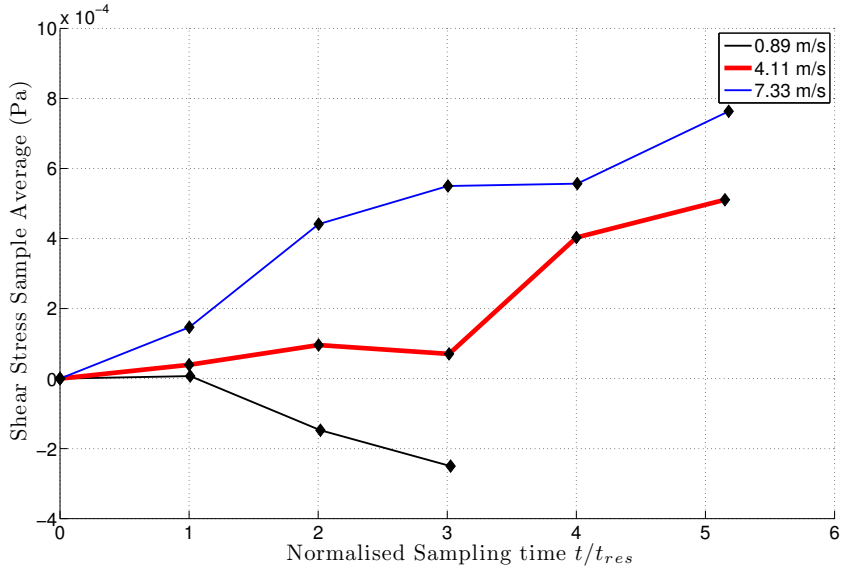

Figure 4.7: Shear Stress Sample Average vs Normalised Sampling Time

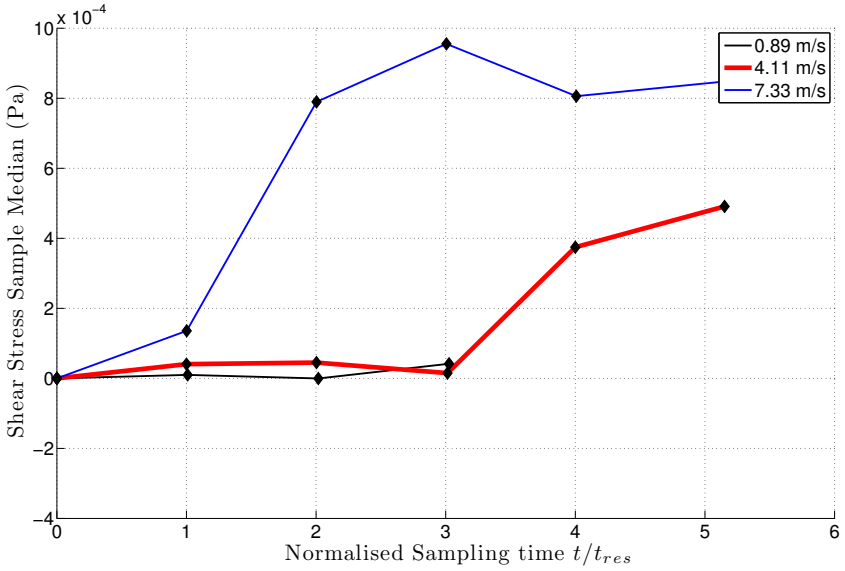

Figure 4.8: Shear Stress Sample Median vs Normalised Sampling Time

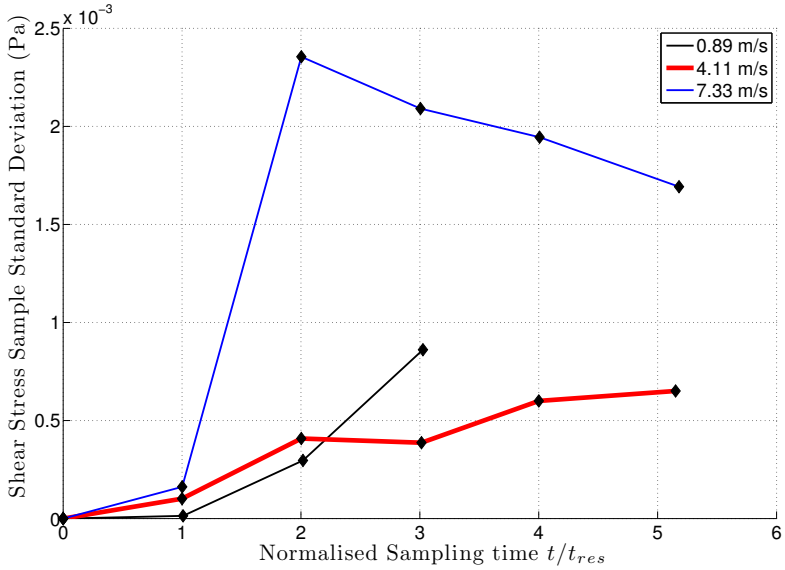

Figure 4.9: Shear Stress Sample Standard Deviation vs Normalised Sampling Time

4.1.5 One-Way ANOVA Test Summary

Table 4.1 and 4.2 summarise the one-way ANOVA test and multiple comparison test results for the samples collected under each wind speed. For all wind speeds, the probability p-values are all much less than the adopted significance level of 0.05. This suggests that at least one of samples in each group has a mean that is not from the same population density function as the other wind speeds. This is conformed in Table 4.2, where a number of samples means for each wind speed are statistically significant from other sample means. The sample number in Table 4.2 corresponds to whether a sample was the first, second, third, fourth or fifth sample collected under each wind speed, as appropriate. Full one-way ANOVA and multiple comparison test results are shown in Appendix E.

Table 4.1: One-Way ANOVA Test Summary

Wind Speed (m/s)	F	Prob > F
7.33	3.08E+00	1.56E-02
4.11	4.27E+01	4.53E-33
0.89	1.22E+01	6.57E-06

Table 4.2: Mean Multiple Comparison Test Summary

Wind Speed (m/s)	No. Samples	Samples with Significant Mean Δ
7.33	5	$1 \neq 5$
4.11	5	1, 2, 3 $\neq$ 4; 1, 2, 3 $\neq$ 5
0.89	3	$1 \neq 2, 3$

4.1.6 Kruskal-Wallis Test Summary

Table 4.3 and 4.4 summarise the Kruskal-Wallis test and multiple comparison test results for the samples collected under each wind speed. For all wind speeds, the probability p-values are all much less than the adopted significance level of 0.05. This suggests that at least one of samples in each group has a median that is not from the same population density function as the other wind speeds. This is conformed in Table 4.4, where samples medians for each wind speed are observed to be statistically significant from other sample medians. The sample number in Table 4.4 corresponds to whether a sample was the first, second, third, fourth or fifth sample collected under each wind speed, as appropriate. Compared with the one-way ANOVA results, the 4.11 m/s sample identified the same samples as being statistically significant. The median has no dependence on outlier values, unlike the mean. Full KW test and multiple comparison test results are shown in Appendix E.

Table 4.3: Kruskal-Wallis Test Summary

Wind Speed (m/s)	Chi-sq	Prob > Chi-sq
7.33	4.63E+01	2.11E-09
4.11	1.23E+02	.92E-26
0.89	5.91E+00	5.20E-02

Table 4.4: Median Multiple Comparison Test Summary

Wind Speed (m/s)	No. Samples	Samples with Significant Median Δ
7.33	5	$1 \neq 2, 3, 4, 5$
4.11	5	$1, 2, 3 \neq 4$; $1, 2, 3 \neq 5$
0.89	3	$2 \neq 3$

4.1.7 Aggregated Non-significant Shear Stress vs Wind Speed

Figure 4.10 shows the aggregated average non-significant shear stresses plotted against wind speed. The 0.89 m/s was approximated as zero based upon the median shear stress at this wind speed. The negative skew was solely caused by a propagating wave entering the sampling zone. The 4.11 m/s and 7.33 m/s samples had successively higher instantaneous shear stresses of 0.00046 and 0.00058 Pa, which reflect the wavs propagating into the sampling region from both directions. These results show that an increase in wind speed results in an increase in instantaneous shear stress, which could break a monolayer coverage up. The relation between wind speed and instantaneous shear stress is non-linear in Figure 4.10. Additional sampling would be required within the wind speed limits before an appropriate function could be fitted to describe the relation between these variables.

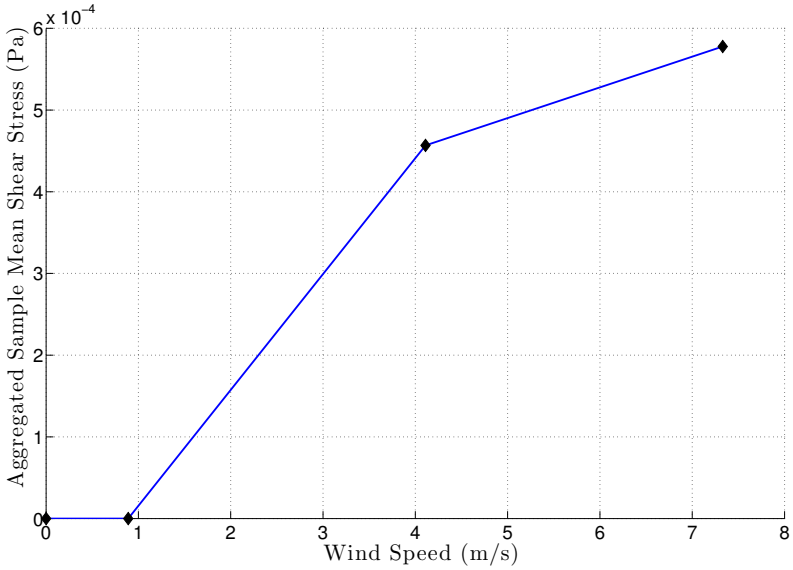

Figure 4.10: Aggregated Non-significant Shear Stress (Pa) vs Wind Speed (m/s)

4.2 Comparison of Results with Previous Studies

Whether the resulting shear stresses of 0 Pa at 0.89 m/s and and 0.00058 Pa at 7.33 m/s are reasonable approximations of the water surface shear stress cannot be determined from this study. Despite this, a trend of increasing shear stress with wind speed was observed and this agrees with the general observation that monolayer performance decreases with increasing wind speed until some threshold (Brink 2011, Palada et al. 2012). the shear stress indicates the development of surface roughness, which could distort and break up a monolayer. At higher wind speeds, the water surface has a larger surface area exposed to the atmosphere due to the wave field distortion, hence, the area for evaporation is increased under a wave field, relative to a calm surface. It would be considered unlikely that 0.00058 Pa would be representative of a typical maximum shear stress as a grid independence study was not completed, the inlet boundary conditions were over-simplified and the fetch over which the wind blows was also limited to 15 m. In practice, much large distances in water reservoirs would likely be observed. Furthermore, the wave field properties of wave height, wavelength and frequency need to be compared with a typical wave field produced, either from a real dam or a laboratory study, to determine if the waves in this model are reasonably representative of waves

which may occur on a water reservoir. Palada et al. (2012) reported wind speeds on 1.3 m/s as the maximum effective wind speed for an octadecanol monolayer. This limit cannot be directly compared with the results of this study, as a wave paddle was not used to introduce waves 2 millimetres in height with a 6 s period.

4.3 Expected and Unexpected Results

A number of results from this study were expected, and a few results were unexpected. Expected results include an increase in the average shear stress with wind speed magnitude, the variability of sample shear stresses and the difference in the velocity gradients between the air and water phases. Unexpected results include failure to converge to a steady state, the development of large waves only at the inlet and the outlet and the standard deviation of the 7.33 m/s sample increasing and then decreasing.

An increase in the average shear stress with wind speed magnitude was expected. This makes sense as higher wind speeds impart greater energy to the water surface, resulting in the development of a more complex wave field. Complex wave fields in a closed basin will have more distortion of the water surface and consequently greater shear stresses. The variability in the shear stresses within a sample was expected. When sampling from irregular wave field, the velocity gradients will be variable throughout the computational domain and subsequently the shear stresses derived will be variable. The velocity gradients in the air phase were expected to be substantially higher than those observed on the water phase. The density and dynamic viscosity of water is a factor of approximately one thousand times greater than that of the air, therefore, the rate of deformation of water will be substantially less than in air for the same energy input or forcing.

It was expected that the sample means for a particular wind speed would converge to a steady-state condition. Evidently, the run time for the simulations was not sufficient to enable steady-state conditions to be reached. It was not expected that large waves would only be generated at the inlet and outlet and that these would propagate into the sampling region. Wind wave theory suggests that waves should develop along the

water surface under a given wind field. The large wave development may be erroneous and the result of poor boundary condition establishment. Furthermore, it was not expected that the standard deviation for the 7.33 m/s wind speed would increase and then decrease. This is likely to be the result of the waves generated at the ends of the computational domain not being superimposed when the second sample was taken. Subsequent superposition produced smaller amplitude waves. Alternatively, as the mean of the sample increased, the separation of observations from the mean decreased; hence, a reduction in the standard deviation.

The significance of the results is that CFD has been use to quantify shear stress over the observed range of monolayer performance for reducing evaporation. The behaviour of the shear stresses appears to be generally consistent with what would be expected. There is an increase in shear stress with an increase in the wind speed. The shear stresses determined are only considered applicable for the computational domain specified in this study. Further refinement of the model, extended simulations and validation will likely yield more accurate instantaneous shear stresses from which to further quantify monolayer performance under wind action. The examination of instantaneous shear stresses under a range of different geometries and different fetch scenarios will identify the range of shear stresses over which monolayers could be considered successful. If the surface average instantaneous shear stress, which represents the distortion of the water surface is known for a proposed reservoir, then through identification of shear stresses under typical wind loading at this site, and comparison with the stresses under which monolayers have been identified as being successful operating under, the expected performance of a monolayer product may be determined.

4.4 Remaining Work, Limitations and Further Work

This section discusses the remaining work to be completed, the limitations of the current study and suggestions for future work.

4.4.1 Remaining Work

Remaining work includes extending the run time of simulations to collect further samples, investigation of the scale-up applicability of the wind-wave results and an investigation of the effect of bank slope on the reflection of waves and the resultant wave field.

As definite convergence of sample mean and median results was not observed in this study, further samples are necessary to confirm that steady-state conditions have been reached under a constant wind. Although steady state conditions should occur in the model used in this study, steady-state conditions are unlikely to occur in a natural basin due to the chaotic nature of wind. In addition to the visual inspection of instantaneous shear stress plots, both ANOVA and KW tests would be employed to investigate whether convergence has achieved. The difference in sample means and medians should not be significant if convergence has been reached.

Investigation of the scale-up applicability of results is required where the size of a real dam under investigation is too large to be replicated in a numerical model. This study used a two-dimensional domain which could be completely modelled. Relatively large or complicated basins will be restricted by the mesh resolution and total number of nodes required to adequately model the reservoir. Similitude, as used with physical models, may be employed to scale a larger dam for numerical modelling purposes. In such cases, geometric, dynamic and kinematic similarity must be satisfied as far as practicable. Alternatively large dams could be subdivided into smaller domains for analysis, provided the boundary conditions are adequately established. A thorough review of similitude and the use of sub-domains is required to satisfy this objective.

The slope of the banks of a dam will result in incident waves being partially or fully reflected in a closed basin. Reflected waves will superimposed with waves generated under wind action sooner in a smaller dam; hence, the surface geometry of a dam will influence the behaviour of waves generated and subsequently the resulting shear stresses. It may even be possible for standing waves to be generated. The remaining work would involve a review of literature for the effect of bank slope on wave reflection and the comparison of four bank slopes: 90°, 60°, 30°, 5°, for the geometry considered

in this paper.

This remaining work and the completed study are subject to a number of limitations.

4.4.2 Limitations of Current Study

There are a number of limitations to this study which affect the accuracy of the results. These limitations include: grid resolution, boundary conditions, turbulence model, two dimensional geometry, temperature, cell-centred nodes, simulation run-time and volume of fluid method. These limitations are not all-inclusive; however, they do represent some of the major limitations affecting the results. Furthermore, despite these limitations, as validation of the model was not undertaken, the degree to which the model results deviate from actual results is unknown.

A grid independence study was not completed; hence, the mesh resolution may not be appropriate to resolve the flow adequately. It has not been established whether or not the grid of 0.025 m will produce different flow field results to a grid of a smaller resolution. For a preliminary study, the grid of 0.025 m was considered sufficient due to constraints on time to collect samples. Refinement of the mesh produce longer computational run times. The grid resolution does not permit a monolayer, one molecule thick, to be included in the model.

The boundary condition at the inlet was simple and not reflective of a real wind field. The wind velocity profile did change from a uniform profile due to the presence of the water surface and the roof of the model, as expected and this is indicated by the velocity gradients. This inlet profile would be irrelevant once steady-state conditions are reached; however, the time to reach steady state conditions may be affected. Furthermore, the uniform velocity boundary condition resulted in waves being generated in the tank. Under a different wind profile, the development of these waves may be different, which will affect the shear stresses generated.

The $k - \varepsilon$ turbulence closure model was considered acceptable for use based on a previous study by Bakhtyar et al. (2010). Different turbulence models were not examined to determine whether the flow field results vary significantly between models. Further-

more, the default initial TKE and Turbulence Dissipation Rates were used. For a real dam, these default values may not be appropriate. For this preliminary investigation, these were considered to be acceptable.

The geometry was constrained to a 15 m by 0.85 m two-dimensional tank. The results are considered to be only applicable for this particular geometry. The use of a longer fetch will likely produce different results due to the delay in the reflection of waves. No account of three-dimensional flow was considered. Although wave motion will generally propagate in the direction of wind, direction variation can result in a wave field that is significantly from that of the two dimensional tank, which produces a different shear stress distribution; hence different disruption of monolayer coverage.

The default values of water density and dynamic viscosity were used in this study. These two properties vary with temperature. The variability in daily and seasonal temperatures due to weather and location means that the observed results may not be appropriate for all sites and at all times of the year.

Node-averaged not node-centred flow field values were examined. The averaging process spreads the volume fraction over various cells vertically and horizontally, diffusing the volume fraction beyond what is necessary. This should be avoided in order to located cells with a volume fraction of one for water, closest to the interface.

The simulation run-time was inadequate to achieve steady state conditions. For the domain used in this study, it was expected that a steady-state condition, where the mean and variance of the shear stress is confined to a limited bandwidth, would be reached. The one-way ANOVA test would show all samples commencing from a steady-state condition having non-significant differences in their means. In practice steady state conditions may not be reached, however over a short time period, it may be reasonable to assume that steady-state conditions would apply. Furthermore, different sampling times will produce different shear stresses. A closer sampling interval may be necessary to remove the possibility that large and small waves are not being hidden through superposition at the sampling times chosen.

The volume of fluid method precludes shear stresses from being computed directly at the air/water interface. This is where the shear stress is desired though. The use of the specific filtering method, where the highest node values in the water phase with a value of one were used to identify velocity gradients, may not be close enough to the interface for adequate representation of the surface shear stress. How close to the interface should be taken as acceptable is another matter not considered, other than as close as possible. The velocity gradients at the air/water interface do influence the velocity gradients in the water below.

Furthermore, as the shear stresses were not validated with experimental data, it is difficult to say with any certainty how far the computed flow field variables differ from what would be observed in an physical model of the tank. Experimentally determining shear stresses would be difficult and/or costly. A monolayer was not modelled. Furthermore, validation of the waves observed, wave height, frequency ad wavelength is required to ensure the waves are representative of wave field properties in a real dam.

Some of the abovementioned limitations can be addressed through refinement of the numerical model.

4.4.3 Suggestions for further work

Considering the significant limitations identified in this study, there is a need to improve the preliminary model. There are many refinements which could be made to the model or further investigations which could be completed. These refinements and additional investigations include: a grid independence study, revision of inlet and roof boundary conditions, turbulence initial conditions, choice of turbulence model, specific filtering region, fitting distributions to the shear stress and wave height, correlating the shear stress with wave height rate of change (vertical velocity), consideration of level set methods, consideration different models to include evaporation, different surface geometry exploration, solver algorithm choice, material properties temperature dependence, surface tension model to possibly include the effects of a monolayer presence, additional wind speeds within region limits, use of a wave paddle, optimising monolayer application and validation options.

A grid independence study is necessary to remove the dependence of the flow field variables on the size of the mesh. The mesh should be sufficiently fine, both overall and in appropriate regions near the interface and the domain boundaries. Additional sample mesh sizes could be 0.05 m and 0.01 m overall. The results for the 7.33 m/s sample could be examined, with further reductions in grid size if necessary. Once independence is seen, the mesh is acceptable for use. This does not mean that the mesh is appropriate, it only means that the flow field results will not be affected by the mesh resolution.

Revision of the inlet and roof boundary conditions are necessary. As the waves are generated in response to the initial wind field, it is necessary that the wind profile be correct. The wind profile used in this study was a uniform profile across the inlet. This profile is not representative of a real wind profile over land, which subsequently passes onto water. The use of a logarithmic profile, or a user defined profile, is appropriate. Furthermore, modification of the roof boundary should be undertaken, as there is no physical boundary in place over a real fluid. The roof should perhaps be substituted with a moving wall with a velocity equal to the mean wind speed under investigation. The use of a roof function would be considered necessary here to prevent wind freely diffusing into the atmosphere; it forces air to flow across the water surface.

The turbulence kinetic energy and turbulence dissipation rates were set to default values. The should be set to match the actual expected conditions. A literature review will be necessary to determine which values would be appropriate for use.

Different turbulence closure models should be investigated. Although the use of the $k-\varepsilon$ model was considered acceptable, there are a number of other models which may yield more accurate results. A literature review would be necessary before examining additional closure models. Alternatively, the Large Eddy Simulation model might be considered. This model differs from the RANS model, as more than one scale of turbulence is considered and the computational requires are substantially higher.

The specific filtering region for the model used was selected as the middle third of the tank. This was considered reasonable as the inlet and outlet conditions were well clear of the sampling region. Consideration should be given to the development length of

the velocity field and the sampling region adjusted if necessary.

Probability density functions should be applied to the instantaneous shear stress relative frequency distributions to see if there is a generally applicable model, at least in the steady-state. This would permit an easy description of the instantaneous shear stress. Wave height density distributions should be fitted with a Rayleigh distribution, which is generally applicable for water waves (Young 1999). Qualitatively, if the distribution fits the Rayleigh distribution adequately, the waves generated by the model could be considered to be acceptable. If the wave height distribution was significantly different from the Rayleigh distribution, this may also be acceptable; however, the model should be checked to see if the wave generation process is appropriate. Probability density functions for shear stress if determined for the computational domain in this study, would be considered acceptable for the study only. The examination of many additional domains sizes would confirm whether the average instantaneous shear stresses are generally applicable. The probability density function of heights does provide a measure of the distortion of the wave surface; however, as shear stress includes velocity gradients it is arguably a better representation of surface distortion for estimating monolayer performance.

A correlation analysis between shear stress and the rate of vertical wave height change (vertical velocity) should be examined. It is expected that there would be a positive correlation between the vertical wave velocity and the shear stress. If there is a positive correlation and it is quantified, then by knowing the instantaneous vertical rate of change in a wave field at a given point, some estimation of the instantaneous shear stress at this point could be made.

Velocity gradients computed from the combined level-set and volume of fluid methods, and the level set method alone, should be compared with the volume of fluid results. This will provide some indication of the velocity gradient variation around the interface.

Consideration should be given to including evaporation in CFD modelling. ANSYS Fluent has an evaporation-condensation model (ANSYS 2011). This model should be reviewed in further detail. The Volume of Fluid model is not included in the evaporation-condensation model, which suggests that interface tracking of wave mo-

tion may be difficult. Perhaps a user defined function could be incorporated in the volume of fluid model, which includes analytic models for evaporation. Water mass could be removed according to an evaporation model.

Different surface geometries should be investigated using a three-dimensional model. Both the directional distribution of waves and the reflection of waves for different surface geometries, under different wind speeds, could be examined. Perhaps some standard charts of maximum wave heights and shear stresses could be produced for various basin sizes. An appropriate range of sizes would need to be examined. This exercise would be very computationally intensive.

The choice of spatial solver algorithms should be reviewed. The second order upwind solvers were considered reasonable for use in this study, as in most cases second order schemes can be used and they are more accurate than first order schemes (ANSYS 2009). If it is appropriate to use another scheme, then this should be investigated.

The air and water material properties should be varied such that fluid flow values reflect different temperature combinations. The macroscopic behaviour of water is unlikely to change too much though.

Surface tension was neglected in this study and no interaction effect was specified between air and water. It may be possible to include the effect of a monolayer on surface tension in the Volume of Fluid model though the use of a surface tension user defined function. The limitations on the accuracy of velocity gradients at the interface, may negate the benefits of using a user defined function.

Additional wind speeds within the generally observed monolayer performance limits could be examined, if only, to provide a better definition of the relationship between wind speed and average instantaneous shear stress.

The use of a wave paddle should be considered. A wave paddle could be set to produce waves of variable wavelength and wave speed, which would result in an irregular wave field. This might be an alternative to using wind over waves. This could simplify the computational requirements significantly. Waves would be drawn from a probability density function for wave height and wave period, which could be completed through

sampling from a specific water basin, or basin of a similar size with similar environmental factors. Monte Carlo simulation could be used to randomly select wave heights from the probability distributions. Further investigation of this option would be necessary. The range of wind speeds for which the probability density function of waves heights was deduced from would need to be known.

Knowledge of monolayer shear stresses will assist in optimising the application of monolayers. If the distortion of the surface is quantified, then monolayer application may be optimised. Particular monolayer products may be developed to suit reservoirs with particular shear stress distributions. Further investigation is required here.

Finally, validation of the model is necessary. Some options for the validation include: the use of particle image velocimetry (PIV) in with a physical model to investigate the instantaneous velocities under waves. CFD models could be devised to replicate these results. Veron et al. (2007) used PIV to study the shear stress in the air over waves. Furthermore, comparison of numerical model wave height distributions with those of an experimental model would also aid in validating a numerical model. Wave height validation would not guarantee that the shear stresses are accurate though.

4.5 Summary

Chapter 4 has presented the results of applying the methodology listed in chapter 3. The results are generally consistent with what would be expected of shear stress under the behaviour of increasing wind speed. An increase in wind speed produces an increase in the shear stress. 0.00058 Pa as reported as the maximum average instantaneous shear stress in this study. The model developed provides a foundation on which advanced models can be developed and additional geometries explored to quantify instantaneous shear stress at monolayer performance limits. A range of water surface geometries and fetch conditions would need to be examined. A reference of instantaneous shear stresses corresponding to operational limits, once compiled, will assist in estimating the likely success of monolayers in a given reservoir. The typical instantaneous shear stresses in a reservoir can be determined from CFD studies.

Chapter 5

Conclusions and Recommendations

5.1 Outcomes of the Current Research

The evaporation reduction capacity of monolayers in a water reservoir is disrupted by the presence of wind-waves. In this study, a multiphase computational fluid dynamics model has been developed to quantifying the water surface stretching, specifically the instantaneous shear stress, in a model air/water reservoir under wind-wave action. Wind speeds corresponding to observed average performance limits of monolayers in reducing evaporation were applied.

The lower wind speed of 0.89 m/s corresponds to the commencement of monolayer transport. The upper limit of 7.33 m/s corresponds to a threshold above which monolayer performance in reducing evaporation is generally negligible. The average of these limits was applied to determine if the relationship between wind speed and average instantaneous shear stress is linear.

The study found that the behaviour of shear stress matched the expectation that shear stress would increase with increasing wind speed and that development of shear stress is quicker for higher wind speeds. For the lower limit wind speed, an average instantaneous

shear stress of zero was found to be valid. For the maximum wind speed, 7.33 m/s, an average instantaneous shear stress of 0.00058 Pa was determined. The shear stress of 0.00046 indicates that the association between wind speed and instantaneous shear stress is non-linear.

Due to the many simplifying assumptions, the average instantaneous shear stresses are considered indicative at best. Limitations, including lack of a grid independence study, simulation run time not reaching steady-state conditions and the lack of validation of the model, do not permit the quantified average instantaneous shear stresses to be considered accurate.

Further studies, with refinement of the model need to be completed before a reliable indicative shear stresses for monolayers at operational limit wind speeds can be determined. A range of water surface geometries and fetch conditions need to be examined. A reference of instantaneous shear stresses corresponding to operational limits, once compiled, will assist in estimating the likely success of monolayers in a given reservoir. The typical instantaneous shear stresses in a reservoir can be determined from CFD studies. Furthermore, knowledge of monolayer shear stresses will assist in optimising the application of monolayers.

The development of this preliminary model and the reporting of average instantaneous shear stress behaviour indicate that the objectives of this project have been satisfied.

5.2 Recommendations for Future Studies

Further work may be classified as either remedial to correct the current model or new where either a new volume of fluid model set up is proposed or a study beyond the volume of fluid CFD model is considered.

Remedial work involves extending the simulation run time until steady-state conditions are reached, completing a grid independence study to confirm whether the grid resolution is appropriate, and investigating the wave height frequency distribution. Steady-state conditions will be indicate by mean and variance which do not have statistically

significant differences between consecutive samples over an appropriate timescale. Grid resolution will be appropriate when the flow field variables are not changing at a given sampling period between progressively smaller grid resolutions. The wave height relative frequency should generally confirm to the Rayleigh distribution function. A correlation between the rate of wave height change (vertical velocity) and shear stress could be conducted.

New volume of fluid modelling work can include any combination of: increasing the number of iterations for the 0.89 m/s sample to 20 to improve the accuracy of solution. Extracting cell-centred flow field values rather than averaged node values. Examination of different turbulence closure models. The use of a moving wall for the roof at a wind speed equal to the mean wind speed. Variation of the Turbulent Kinetic Energy and Turbulence Dissipation Rates rather than using default values. The inclusion of a user defined function at the interface to account for the lack of evaporation in the volume of fluid model, this model could remove water mass from the flow according to a closed form analytical function from relevant literature. Adaptive meshing could be investigated. Surface tension effects could be included, perhaps a user defined function could include the effects of a monolayer on surface tension. The coupling of the level-set interface capturing method with the volume of fluid approach could also be examined.

Further new studies could include: the investigation of the use and applicability of the evaporation-condensation model in ANSYS Fluent. Use of particle image velocimetry (PIV) for validation of water velocity movements and therefor velocity gradients and shear stress. The investigation of a range of surface geometries and fetch lengths and a three dimensional model to include the effects of a wave directional propagation. Monolayer products could be developed to target defined shear stress distributions. The use of a numerical wave paddle which generates random wavelength and amplitude waves from known probability density functions of wave height and period could be considered; sampling could be completed using Monte Carlo methods. Finally, Large Eddy Simulation or Direction Numerical Simulation models could be examined. There are seemingly endless possibilities with CFD provided the time and computational capabilities are available.

References

Anderson Jr, J. D. (1995), *Computational Fluid Dynamics: The Basics with Applications*, McGraw-Hill series in mechanical engineering, McGraw-Hill, Inc.

ANSYS (2009), *ANSYS FLUENT 12.0 User's Guide*, ANSYS Inc.

ANSYS (2011), *ANSYS FLUENT Theory Guide R14*, ANSYS Inc.

Bakhtyar, R., Razmi, A., Barry, D., Yeganeh-Bakhtiary, A. & Zou, Q. (2010), 'Air–water two-phase flow modeling of turbulent surf and swash zone wave motions', *Advances in Water Resources* **33**(12), 1560 – 1574.

Barnes, G. (2008), 'The potential for monolayers to reduce the evaporation of water from large water storages', *Agricultural Water Management* **95**(4), 339 – 353.

BOM (2010), 'Nmoc operations bulletin no. 84: The implementation of the auswave wave model at the australian bureau of meteorology - draft'. Accessed: 10 December, 2012.
URL: *http* : *//www.bom.gov.au/australia/charts/bulletins/apob*84.*pdf*

Brink, G. N. (2011), Universal Design Framework for optimal application of chemical monolayer to open water surfaces, PhD thesis, University of Southern Queensland (USQ).

Coop, P. A., Lamb, D. W., Fellows, C. M. & Bradbury, R. (2011), Automatic detection of evaporation reducing monolayers, *in* 'Proceedings of the Biennial Conference of the Australian Society for Engineering in Agriculture (SEAg)', SEAg, Surfers Paradise QLD.

Craig, I. (2005), *Loss of storage water due to evaporation - a literature review*, NCEA, University of Southern Queensland, Australia.

Craig, I., Mossad, R. & Hancock, N. (2006), Development of a cfd based dam evaporation model, Vol. 2.

CSIRO (2007), 'Climate change in australia: Observed changes and projections summary brochure'. Accessed: 10 December, 2012.
URL: *http* : *//www.climatechangeinaustralia.gov.au/*

Dean, R. G. & Dalrymple, R. A. (1991), *Water Wave Mechanics for Engineers and Scientists*, Vol. 2 of *Advanced Series on Ocean Engineering*, World Scientific Publishing Co. Pte. Ltd., Singapore.

Gerlach, D., Tomar, G., Biswas, G. & Durst, F. (2006), 'Comparison of volume-of-fluid methods for surface tension-dominant two-phase flows', *International Journal of Heat and Mass Transfer* **49**(3), 740 – 754.

Hancock, N. H., Pittaway, P. A. & Symes, T. W. (2011), 'Assessment of the performance of evaporation suppressant films: Analysis and limitations of simple trialling methods', *Australian Journal of Multi-disclipinary Engineering* **8**(2), 157 – 167.

Helfer, F., Lemckert, C. & Zhang, H. (2011), Investigating techniques to reduce evaporation from small reservoirs in australia, *in* 'Proceedings of the 34th IAHR World Congress 33rd Hydrology and Water Resources Symposium 10th Conference on Hydraulics in Water Engineering', Engineers Australia, Brisbane, Australia.

Huang, Y., Zhang, H., j. Lemckert, C. & Schouten, P. W. (2011), Numerical study of the seasonal wave action developed at an agricultural water reserve, *in* 'Proceedings of the 34th IAHR World Congress 33rd Hydrology and Water Resources Symposium 10th Conference on Hydraulics in Water Engineering', Engineers Australia, Brisbane, Australia.

Janssen, P. A. E. M. (2008), 'Progress in ocean wave forecasting', *Journal of Computational Physics* **227**(7), 3572 – 3594.

Lal, A. & Elangovan, M. (2008), 'Cfd simulation and validation of flap type wavemaker', *World Academy of Sciences, Engng. Tech* **46**, 76 – 82.

Lin, M.-Y., Moeng, C.-H., Tsai, W.-T., Sullivan, P. P. & Belcher, S. E. (2008), 'Direct numerical simulation of wind-wave generation processes', *Journal of Fluid Mechanics* **616**, 1 – 30.

McJannet, D., Cook, F., Knight, J. & Burn, S. (2008), *Evaporation reduction by monolayers: overview, modelling and effectiveness*, CSIRO: Water for a Healthy Country National Research Flagship, Urban Water Security Alliance Technical Report No. 6.

Mitsuyasu, H. (2002), 'A historical note on the study of ocean surface waves', *Journal of Oceanography* **58**(1), 109 – 120.

Palada, C., Schouten, P. & Lemckert, C. (2012), 'Testing the effectiveness of monolayers under wind and wave conditions', *Water Science and Technology* **65**(6), 1137 – 1141.

Schouten, P. W., Palada, C., Lemckert, C. J., Sunartio, D. & Solomon, D. H. (2011), Analysis of chemical film monolayers under wind and wave conditions, *in* 'Proceedings of the 34th IAHR World Congress 33rd Hydrology and Water Resources Symposium 10th Conference on Hydraulics in Water Engineering', Engineers Australia, Brisbane, Australia.

Sullivan, P. P. & McWilliams, J. C. (2010), 'Dynamics of winds and currents coupled to surface waves', *Annual Review of Fluid Mechanics* **42**(1), 19 – 42.

Tu, J., Yeoh, G. H. & Liu, C. (2008), *Computational Fluid Dynamics: A Practical Approach*, Butterworth-Heinemann, Burlington, USA.

Veron, F., Saxena, G. & Misra, S. (2007), 'Measurements of the viscous tangential stress in the airflow above wind waves', *Geophys. Res. Lett* **34**, L19603.

Wang, Z., Zou, Q. & Reeve, D. (2009), 'Simulation of spilling breaking waves using a two phase flow cfd model', *Computers & Fluids* **38**(10), 1995 – 2005.

Young, I. R. (1999), *Wind Generated Ocean Waves*, Vol. 2 of *Elsevier Ocean Engineering Book Series*, Elsevier, Oxford.

Appendix A

Project Specification

University of Southern Queensland

FACULTY OF ENGINEERING AND SURVEYING

ENG 4111/2 Research Project

Project Specification

For:	**Edward Stephen GREIG**
Topic:	Numerical Simulation of Water Waves in Reservoirs Affecting Evaporation
Supervisor:	Dr. Andrew Wandel
Enrolment:	ENG4111 - S1, D, 2012 ENG4112 - S2, D, 2012
Sponsorship:	Faculty of Engineering & Surveying National Centre for Engineering in Agriculture (NCEA)
Project Aim:	To undertake a Computational Fluid Dynamics (CFD) study of wave generation by wind in order to investigate the efficiency of monolayers in reducing evaporation from water reservoirs.

Program: **(Issue A, 21 March 2012)**

1. Research wind-wave theory and the numerical modelling of wind-waves.
2. Research evaporation of water from reservoir bodies.
3. Research the effectiveness of monolayers in reducing evaporation under the action of wind-waves.
4. Develop a 2D / 3D Computational Fluid Dynamics (CFD) model for simulating wave generation by wind, incorporating two phases (air/water) in a representative reservoir.
5. Apply the developed CFD model to investigate water surface stretching in response to wave action under defined wind loading scenarios. Validate the model with numerical data from USQ, if available.

6. Critically analyse and discuss the surface stretching response and the implications of wind-waves on monolayer efficiency in reducing evaporation.

7. Investigate the scale-up applicability of the wind-wave results from model output to field trials.

8. Recommendations for further studies.

As time and resources permit:

1. Investigate the effect of reservoir bank slope on wind-wave height resulting from wave reflection.

Agreed:

Student Name:	Edward Greig
Date:	21 March 2012
Supervisor Name:	Dr. Andrew Wandel
Date:	21 March 2012
Examiner/Co-Examiner:	Mr. Chris Snook
Date:	

Appendix B

Flow Field Phase and Horizontal Velocity Gradient Contour Plots

B.0.1 Introduction

Appendix B contains CFD phase and Horizontal Velocity Gradient plots. These provide a visual indication of surface deformation under wind loading over the region 5 to 10 m from the inlet.

B.0.2 7.33 m/s Phase Plots

The 7.33 m/s phase plots are shown in Figures B.1 to B.5.

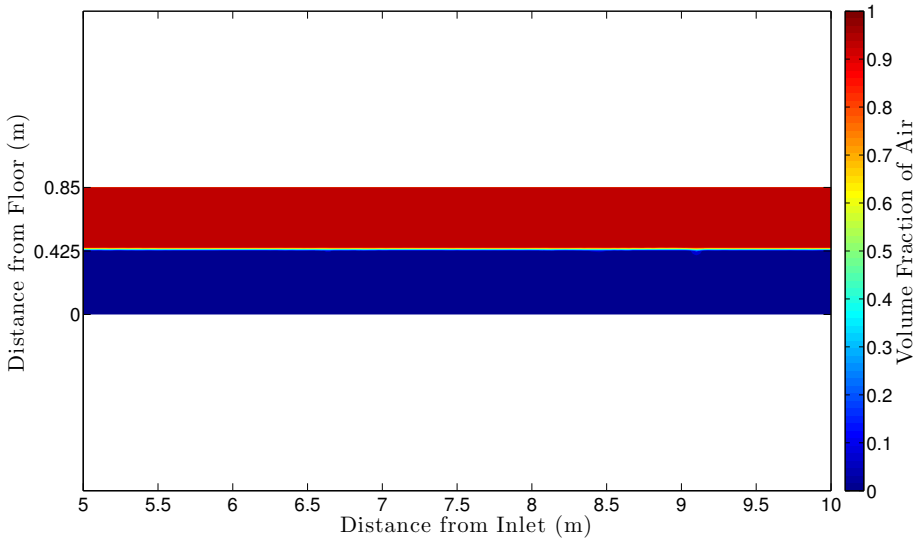

Figure B.1: Wind Speed 7.33 m/s, Phase Plot, 2.05 s

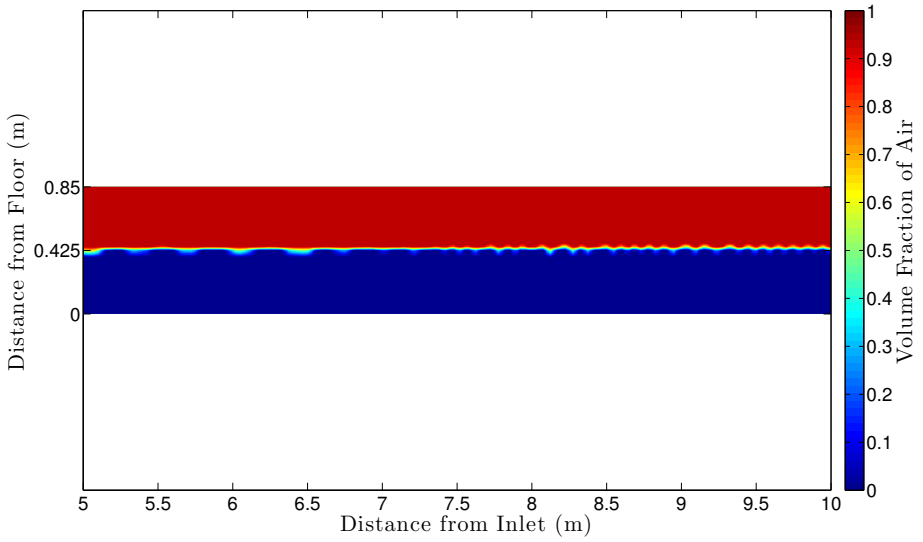

Figure B.2: Wind Speed 7.33 m/s, Phase Plot, 4.10 s

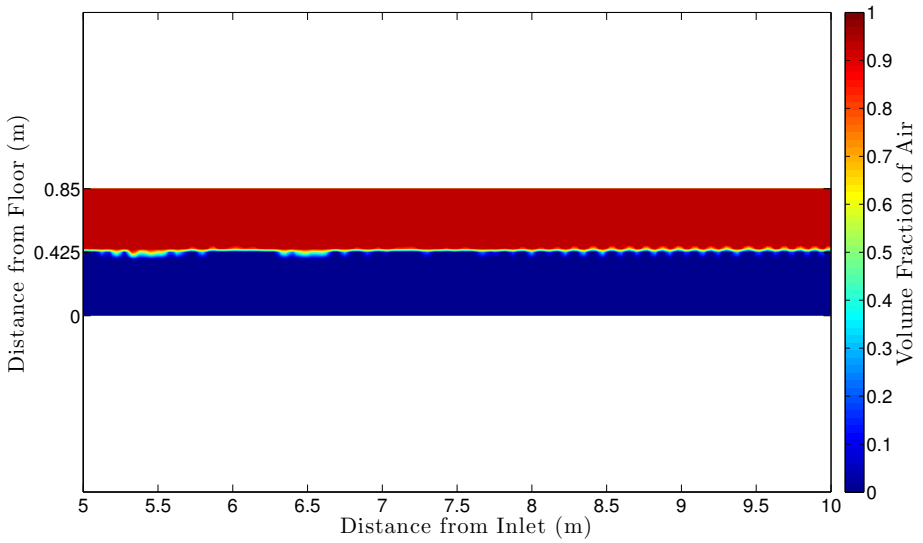

Figure B.3: Wind Speed 7.33 m/s, Phase Plot, 6.15 s

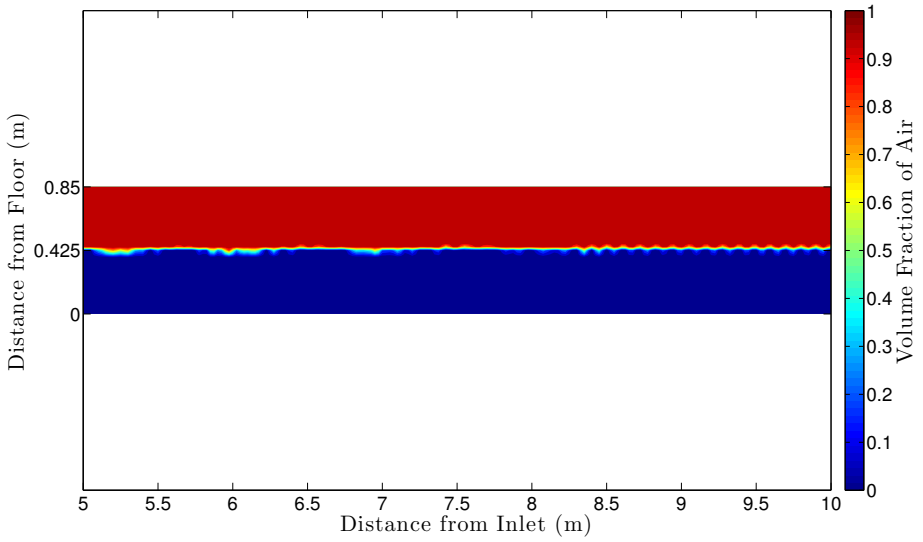

Figure B.4: Wind Speed 7.33 m/s, Phase Plot, 8.20 s

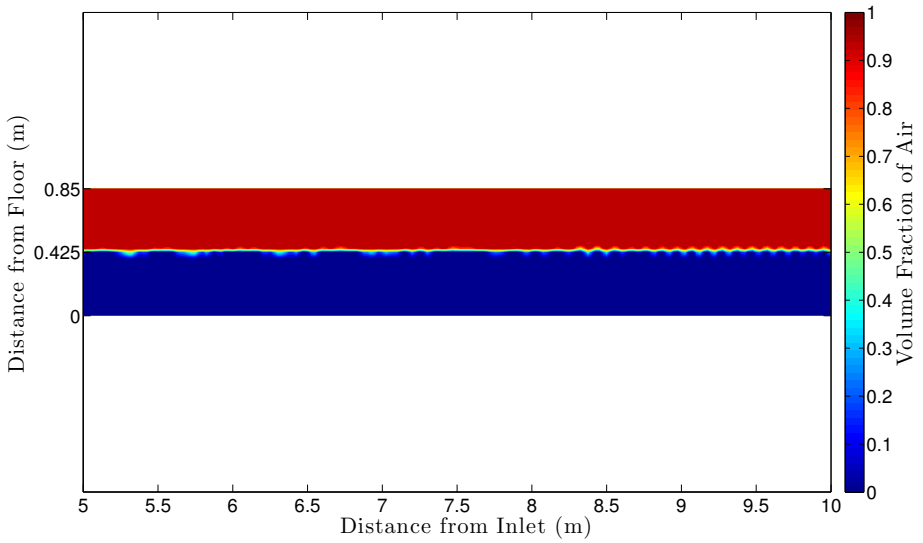

Figure B.5: Wind Speed 7.33 m/s, Phase Plot, 10.6 s

B.0.3 4.11 m/s Phase Plots

The 4.11 m/s phase plots are shown in Figures B.6 to B.10.

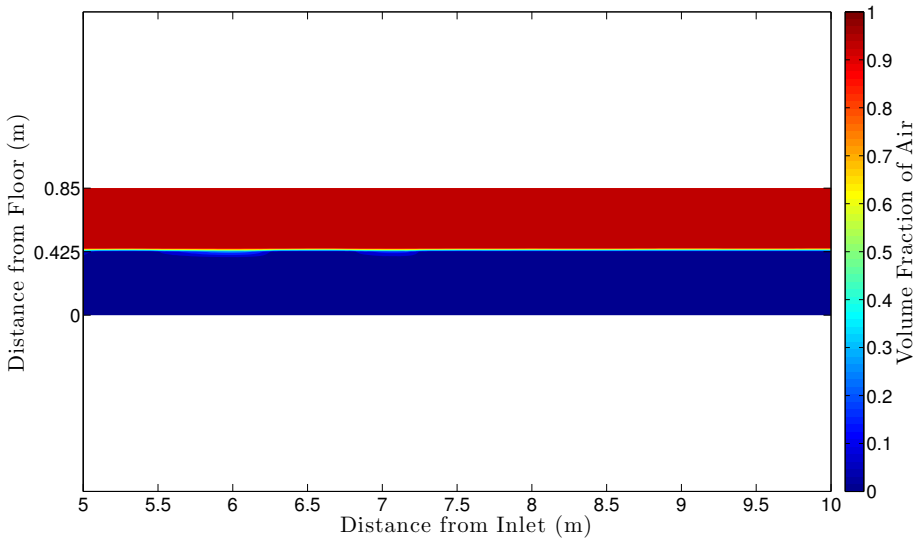

Figure B.6: Wind Speed 4.11 m/s, Phase Plot, 3.65 s

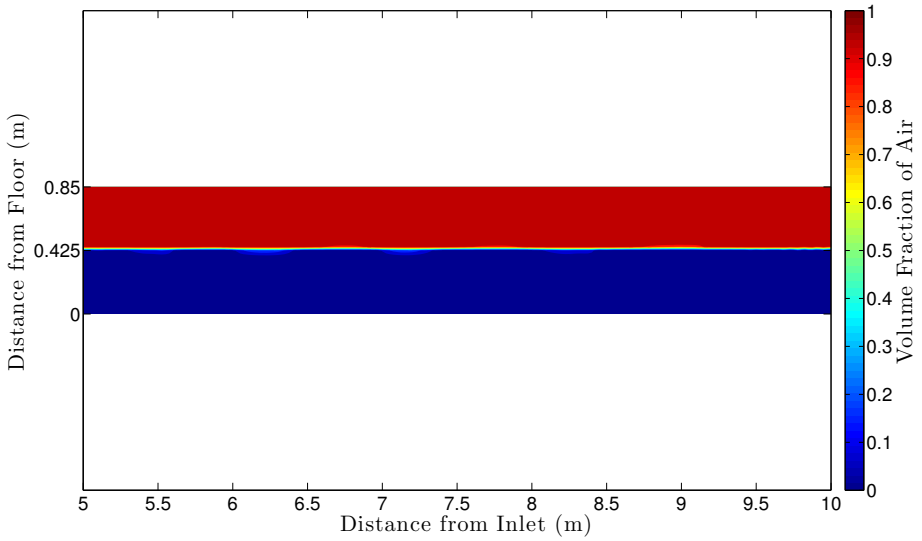

Figure B.7: Wind Speed 4.11 m/s, Phase Plot, 7.31 s

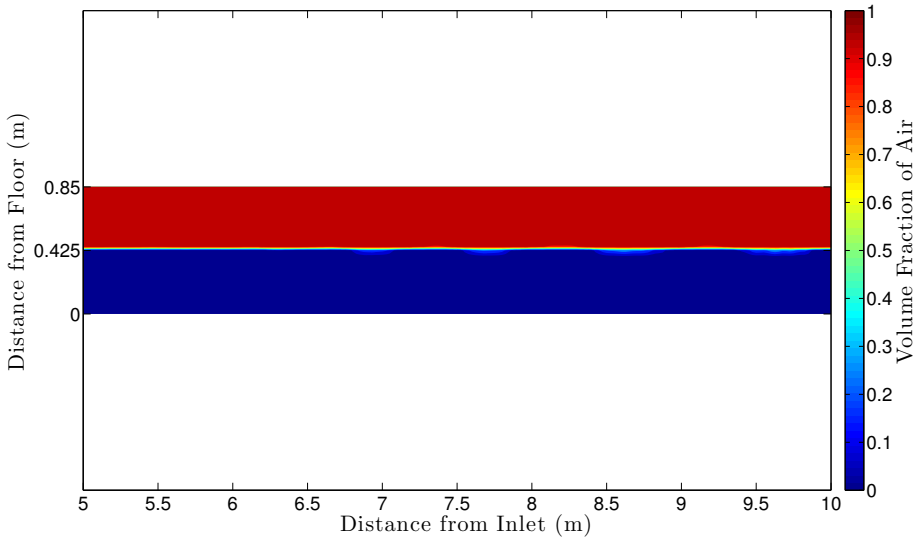

Figure B.8: Wind Speed 4.11 m/s, Phase Plot, 11.0 s

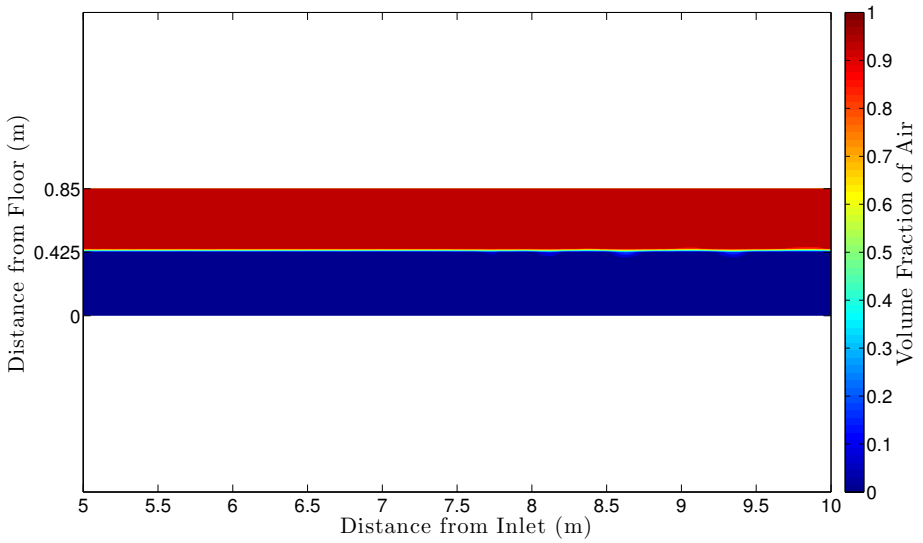

Figure B.9: Wind Speed 4.11 m/s, Phase Plot, 14.6 s

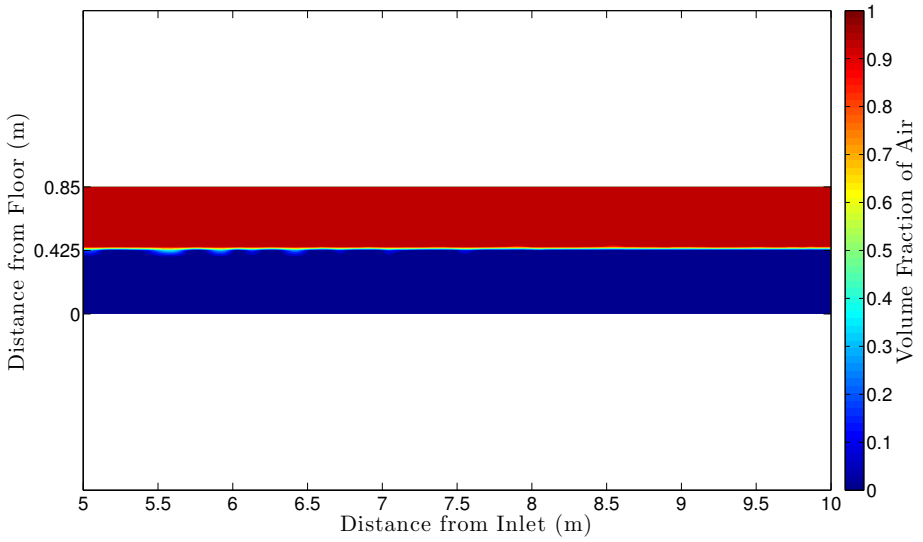

Figure B.10: Wind Speed 4.11 m/s, Phase Plot, 18.8 s

B.0.4 0.89 m/s Phase Plots

The 0.89 m/s phase plots are shown in Figures B.11 to B.13.

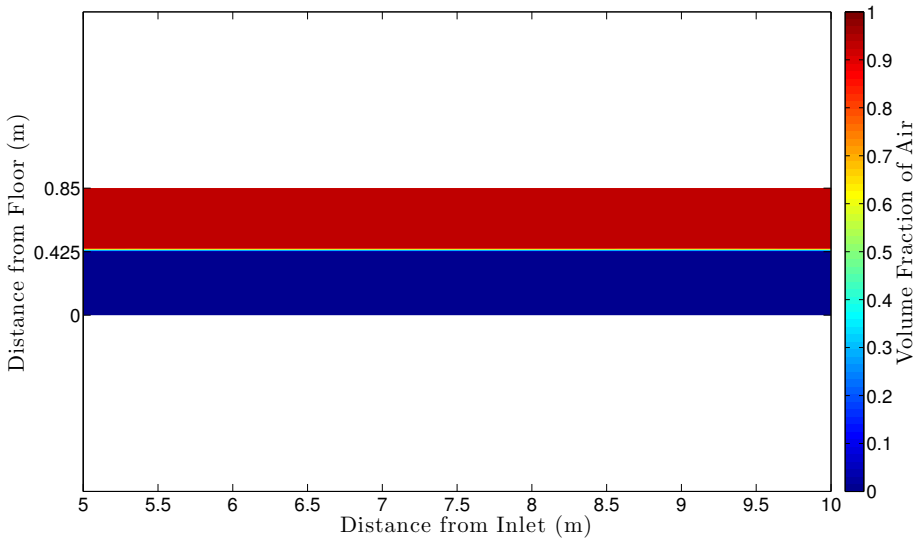

Figure B.11: Wind Speed 0.89 m/s, Phase Plot, 17.0 s

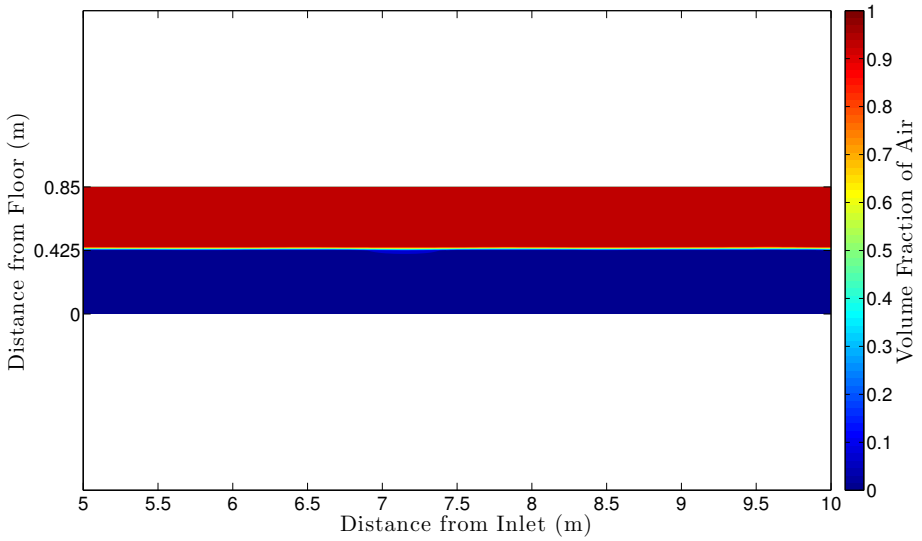

Figure B.12: Wind Speed 0.89 m/s, Phase Plot, 34.0 s

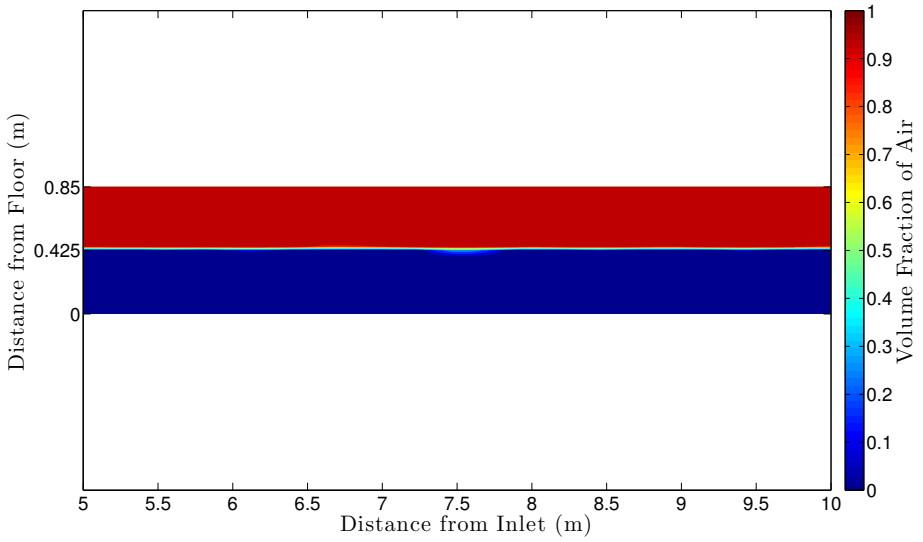

Figure B.13: Wind Speed 0.89 m/s, Phase Plot, 51.0 s

B.0.5 7.33 m/s Horizontal Velocity Gradient Plots

The 7.33 m/s phase plots are shown in Figures B.14 to B.18.

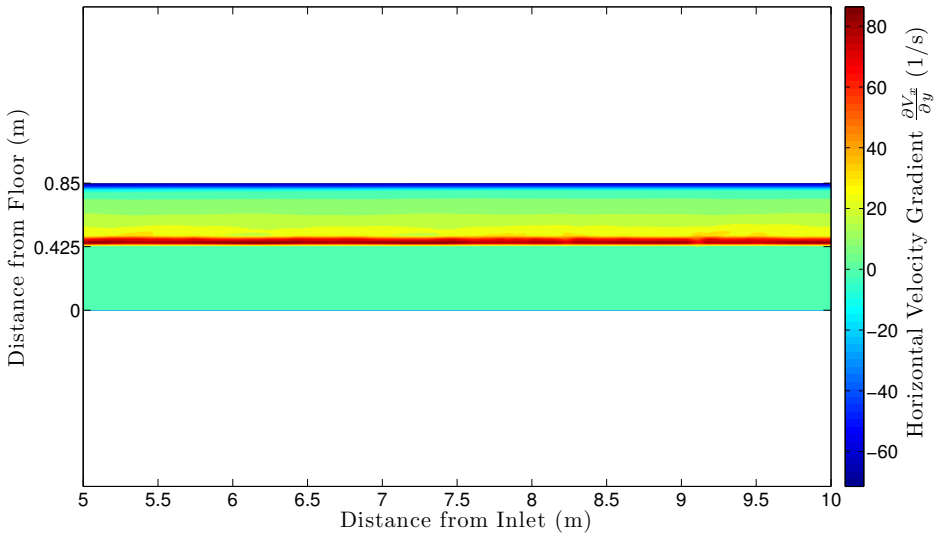

Figure B.14: Wind Speed 7.33 m/s, Horizontal Velocity Gradient Plot, 2.05 s

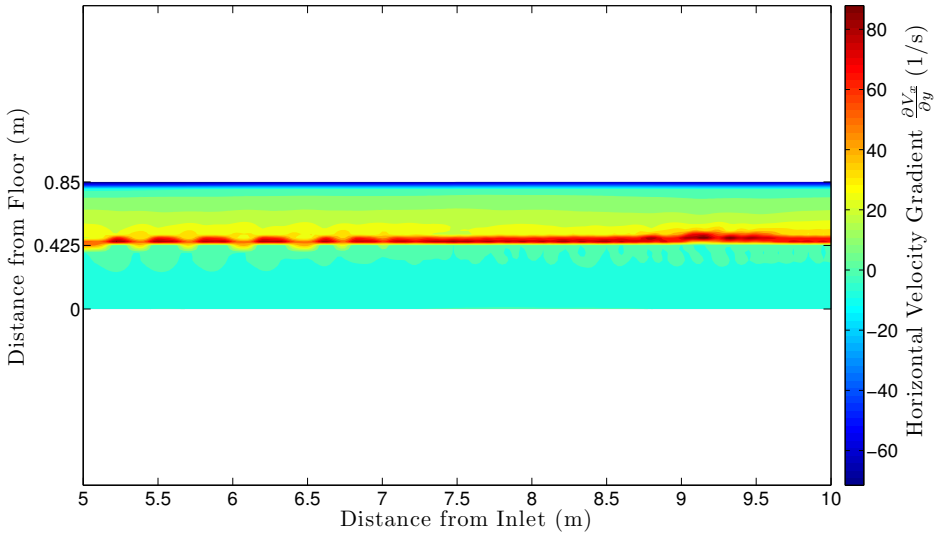

Figure B.15: Wind Speed 7.33 m/s, Horizontal Velocity Gradient Plot, 4.10 s

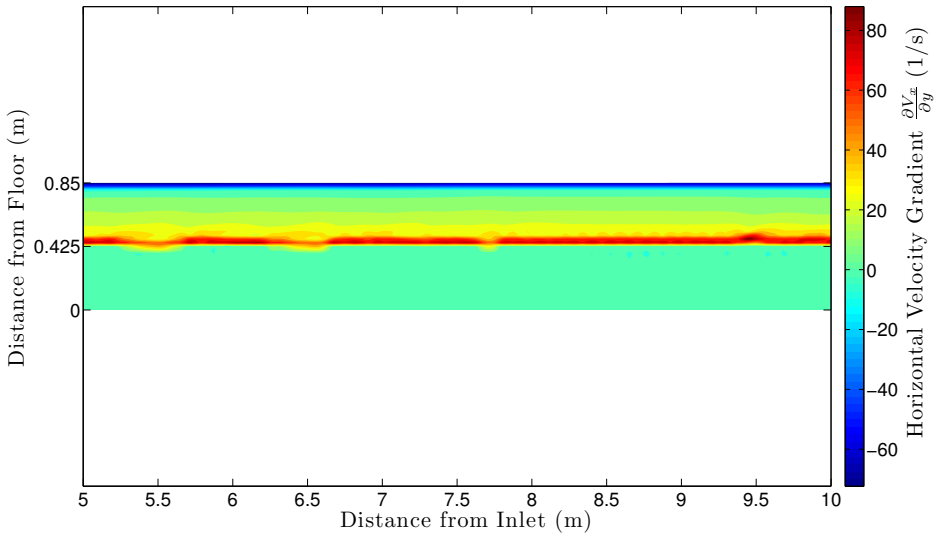

Figure B.16: Wind Speed 7.33 m/s, Horizontal Velocity Gradient Plot, 6.15 s

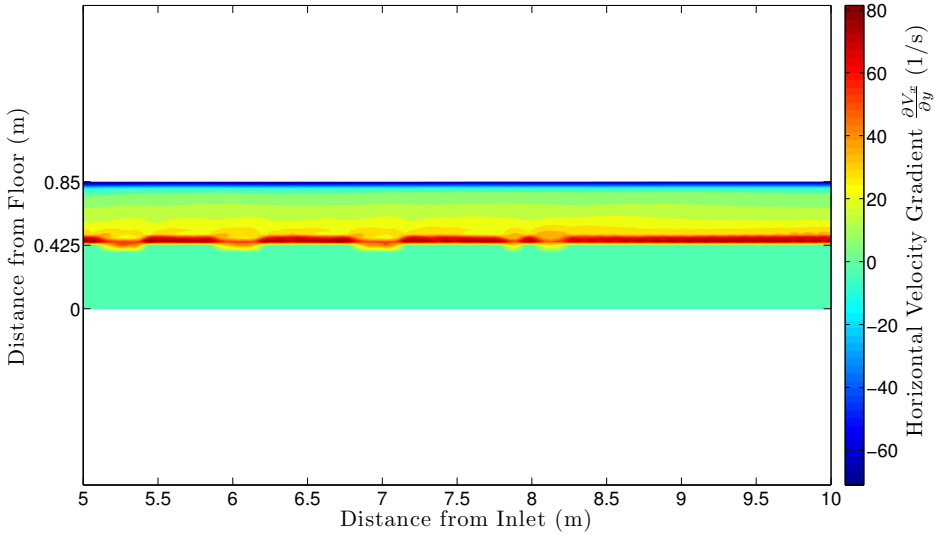

Figure B.17: Wind Speed 7.33 m/s, Horizontal Velocity Gradient Plot, 8.20 s

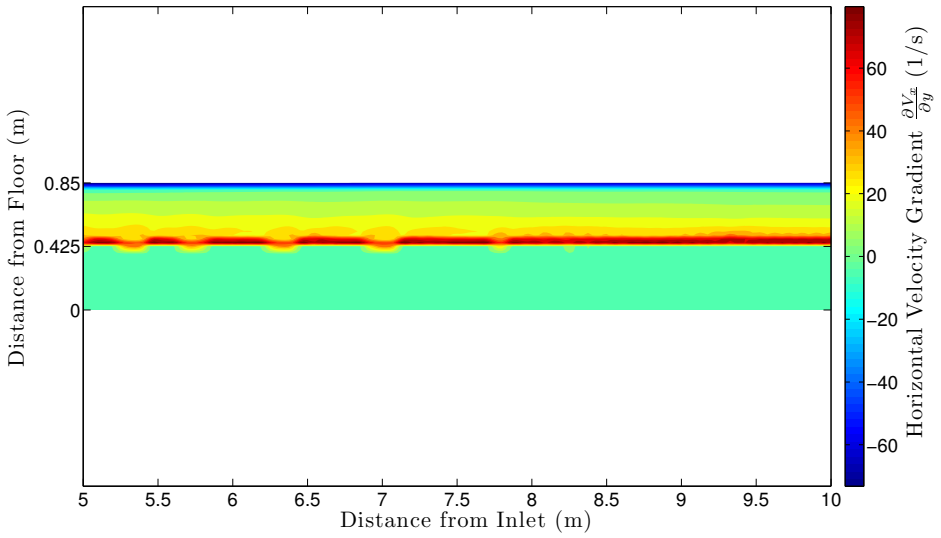

Figure B.18: Wind Speed 7.33 m/s, Horizontal Velocity Gradient Plot, 10.6 s

B.0.6 4.11 m/s Horizontal Velocity Gradient Plots

The 4.11 m/s phase plots are shown in Figures B.19 to B.23.

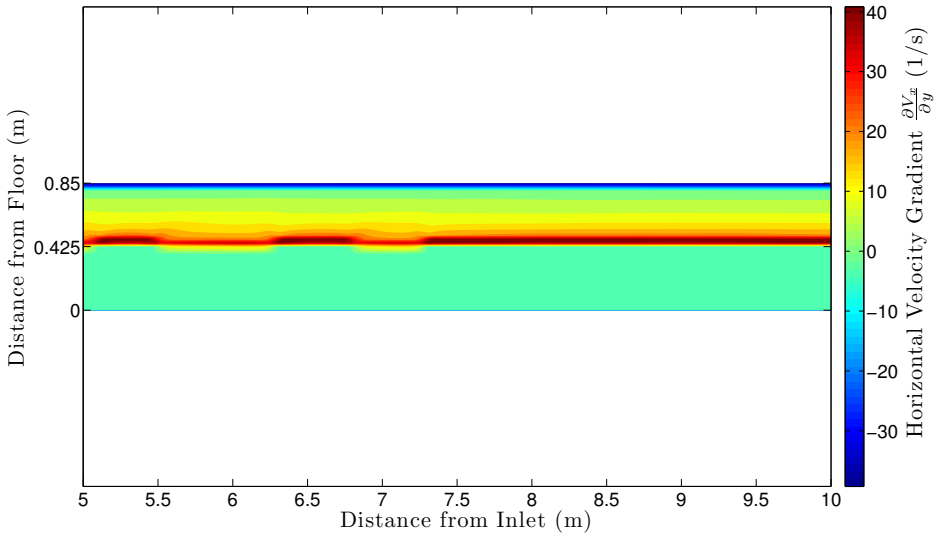

Figure B.19: Wind Speed 4.11 m/s, Horizontal Velocity Gradient Plot, 3.65 s

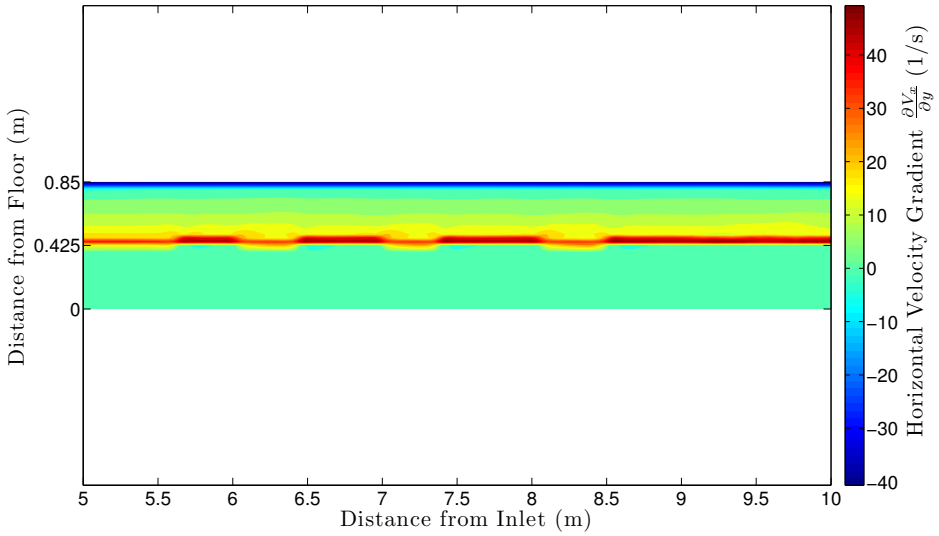

Figure B.20: Wind Speed 4.11 m/s, Horizontal Velocity Gradient Plot, 7.31 s

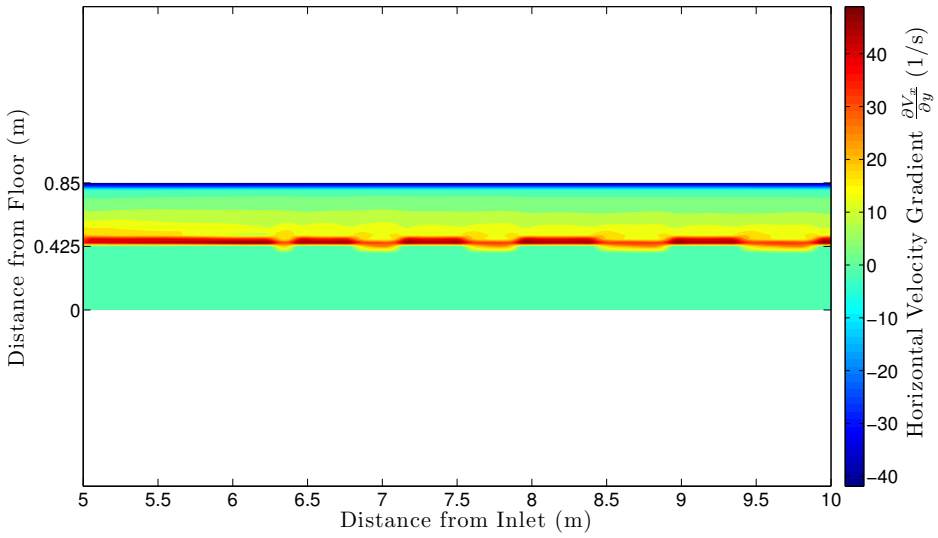

Figure B.21: Wind Speed 4.11 m/s, Horizontal Velocity Gradient Plot, 11.0 s

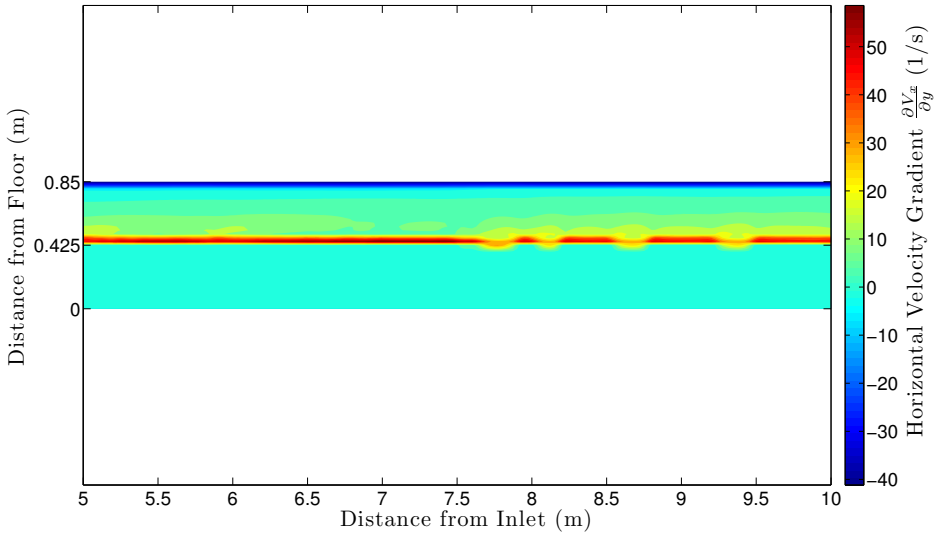

Figure B.22: Wind Speed 4.11 m/s, Horizontal Velocity Gradient Plot, 14.6 s

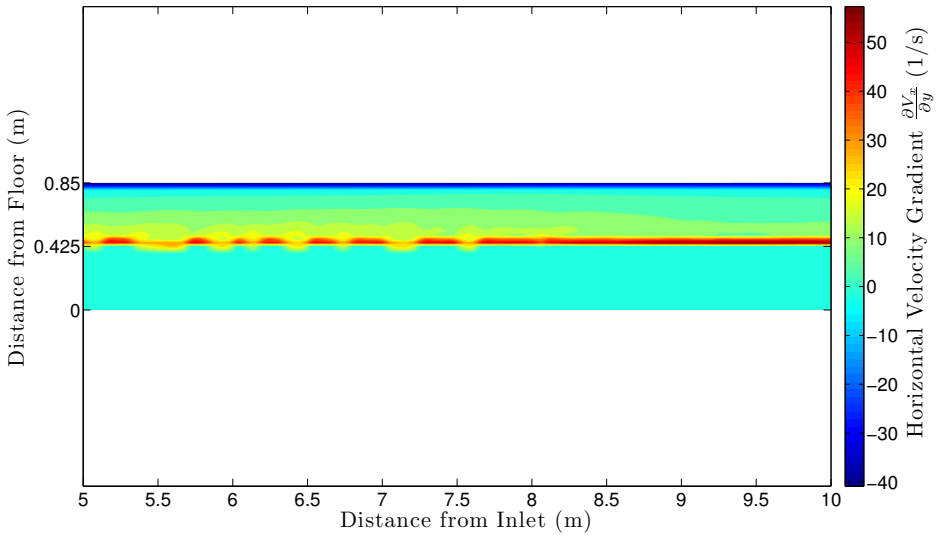

Figure B.23: Wind Speed 4.11 m/s, Horizontal Velocity Gradient Plot, 18.8 s

B.0.7 0.89 m/s Horizontal Velocity Gradient Plots

The 0.89 m/s phase plots are shown in Figures B.24 to B.26

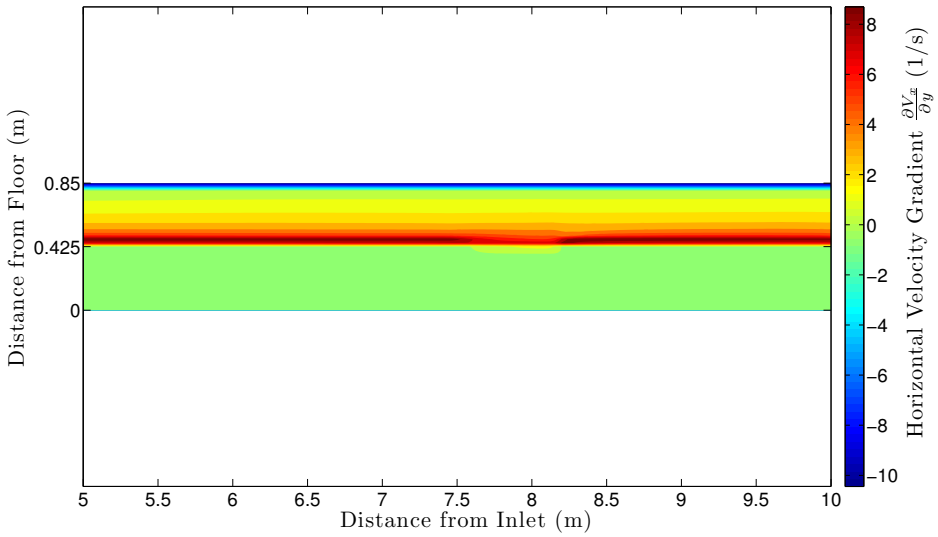

Figure B.24: Wind Speed 0.89 m/s, Horizontal Velocity Gradient Plot, 17.0 s

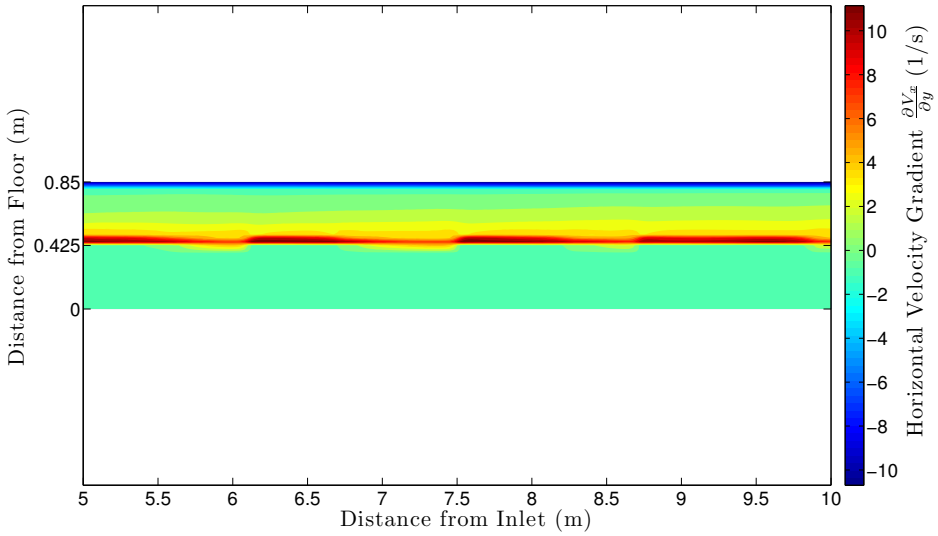

Figure B.25: Wind Speed 0.89 m/s, Horizontal Velocity Gradient Plot, 34.0 s

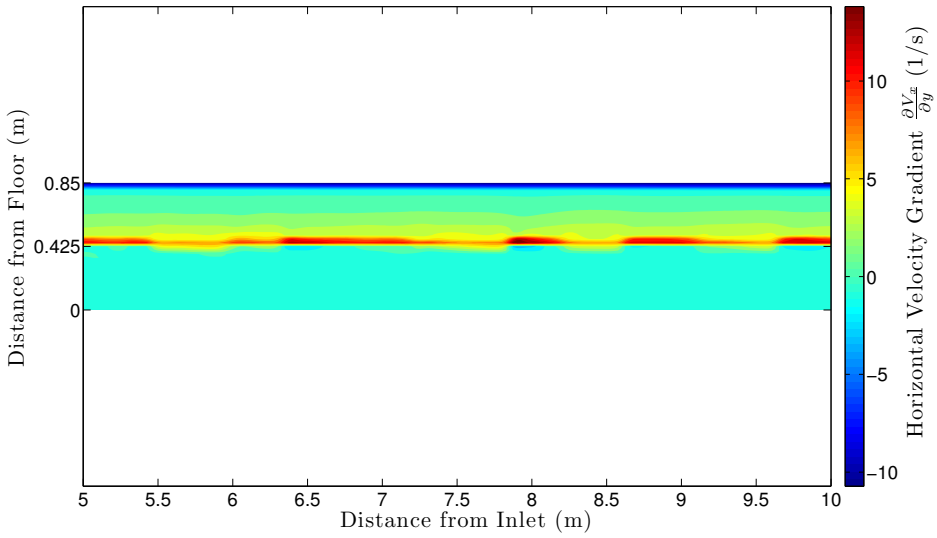

Figure B.26: Wind Speed 0.89 m/s, Horizontal Velocity Gradient Plot, 51.0 s

Appendix C

Sample Shear Stress Profiles

C.0.8 Introduction

Appendix C presents the shear stress profiles for the samples taken from the ANSYS Fluent model in accordance with the filtering method of Section 3.3. These are presented as relative frequency histograms in Appendix D.

Figure C.1 shows the sample shear stress profiles for 7.33 m/s samples:

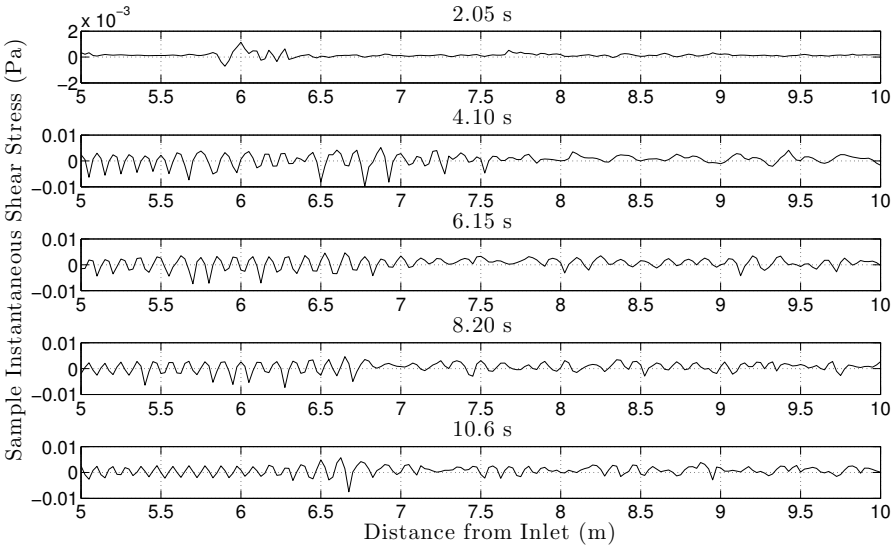

Figure C.1: Shear stress time profilea, wind speed 7.33 m/s

Figure C.2 shows the sample shear stress profiles for 4.11 m/s samples:

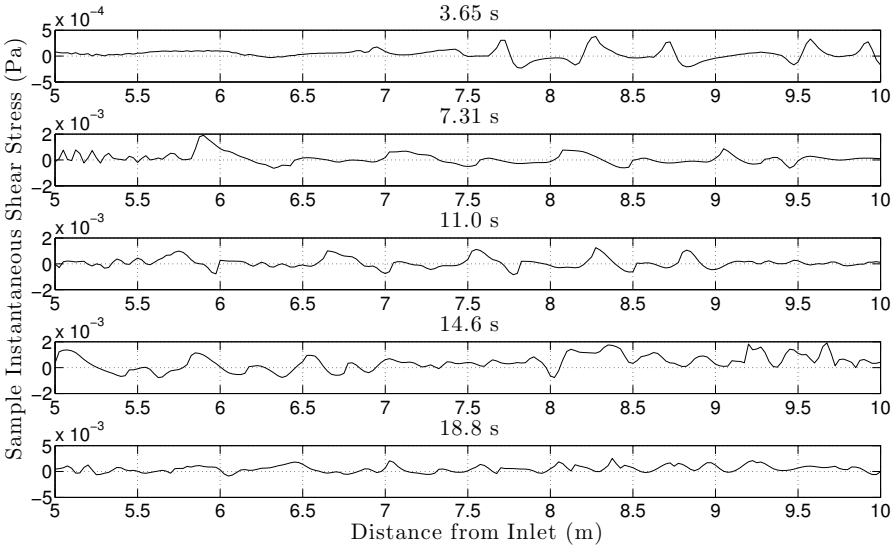

Figure C.2: Shear stress time profilea, wind speed 4.11 m/s

Figure C.3 shows the sample shear stress profiles for 0.89 m/s samples:

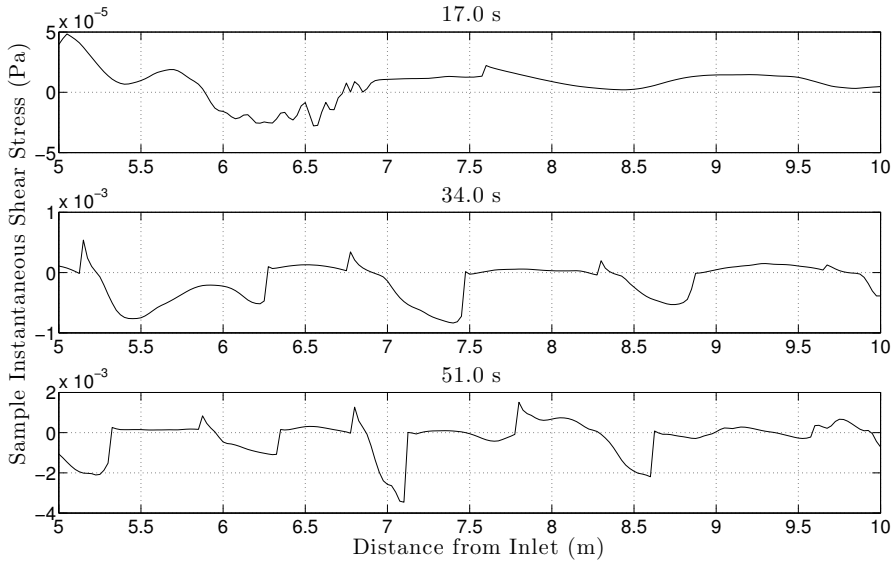

Figure C.3: Shear stress time profilea, wind speed 0.89 m/s

Appendix D

Sample Shear Stress Distributions

D.0.9 Introduction

Figure D.1 shows the shear stress distribution for samples 1 to 3 for 0.89 m/s.

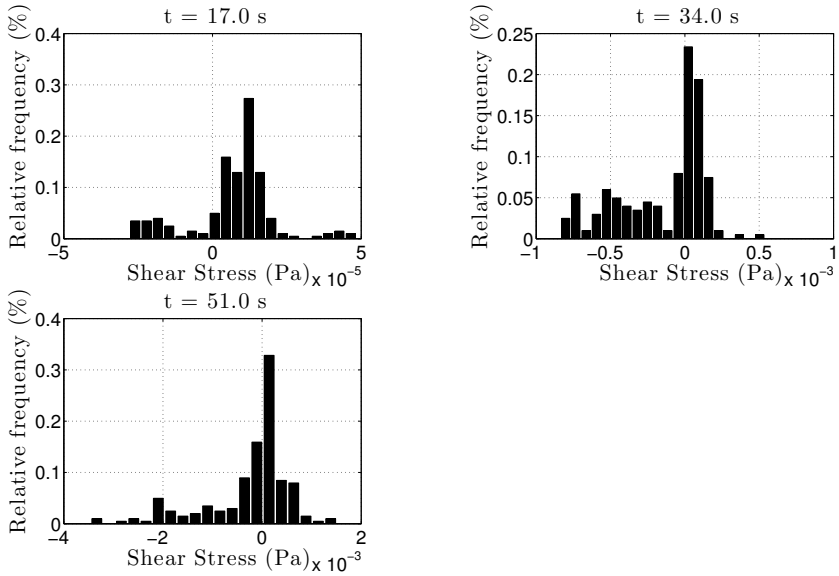

Figure D.1: Shear stress distributions, wind speed 0.89 m/s

Figure D.2 shows the shear stress distribution for samples 1 to 4 for 4.11 m/s. Figure D.3 shows sample 5.

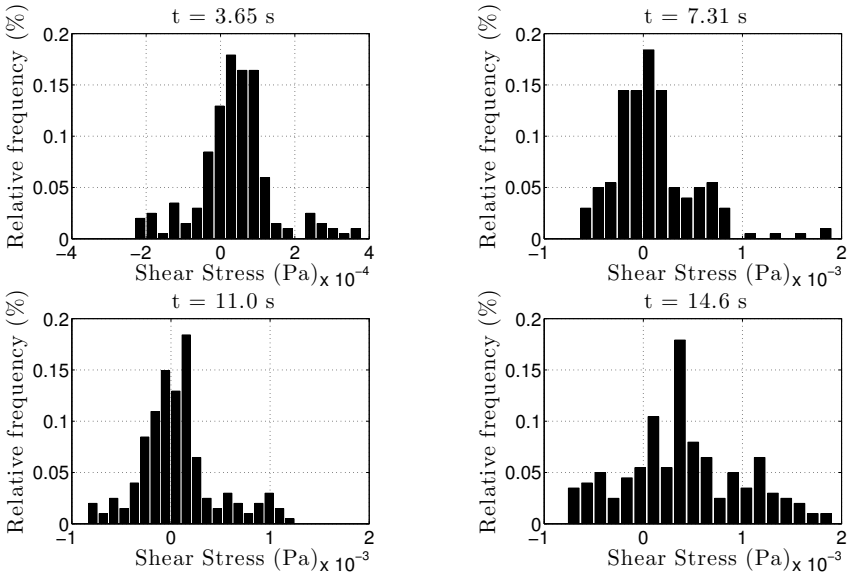

Figure D.2: Shear stress time distributions, wind speed 4.11 m/s

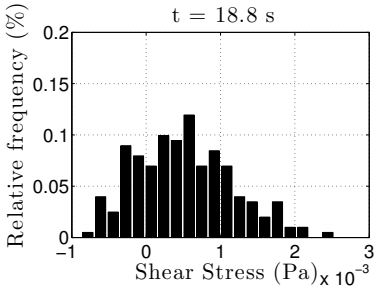

Figure D.3: Shear stress time distributions, wind speed 4.11 m/s

Figure D.4 shows the shear stress distribution for samples 1 to 4 for 7.33 m/s. Figure D.5 shows sample 5.

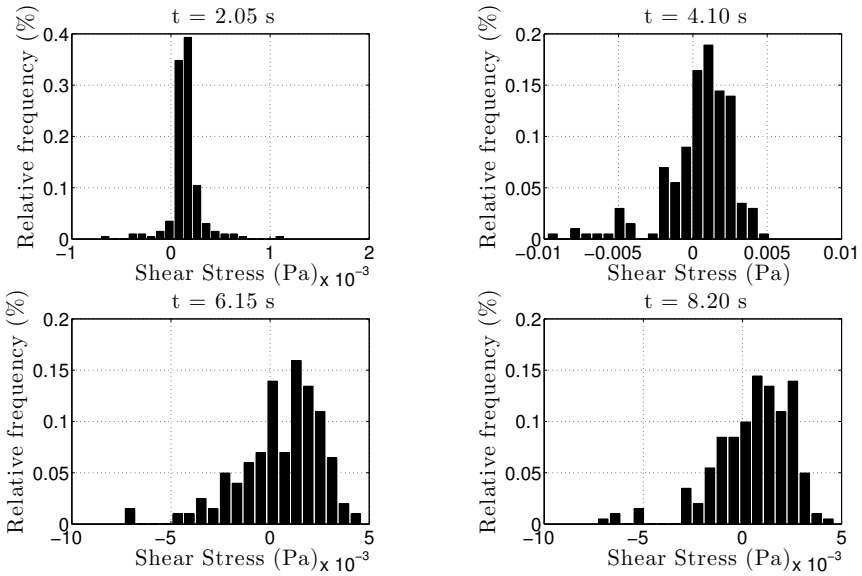

Figure D.4: Shear stress time distributions, wind speed 7.33 m/s

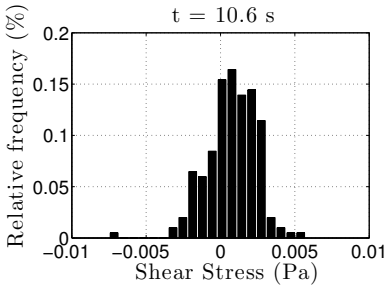

Figure D.5: Shear stress time distributions, wind speed 7.33 m/s

Appendix E

One-way ANOVA, Kruskal-Wallis Test and Multiple Comparison Test Results

E.0.10 Introduction

Appendix C contains the ANOVA and Multiple Comparison Test results as output from the Matlab scripts in Appendix D.

E.0.11 One-Way ANOVA

Table E.1 shows the One-Way ANOVA results for the 0.89 m/s wind speed:

Table E.1: One-Way ANOVA, wind speed 0.89 m/s

Source	SS	df	MS	F	Prob > F
Columns	6.73E-06	2	3.36E-06	1.22E+01	6.57E-06
Error	1.66E-04	600	2.76E-07		
Total	1.73E-04	602			

Table E.2 shows the One-Way ANOVA results for the 4.11 m/s wind speed:

Table E.2: One-Way ANOVA, wind speed 4.11 m/s

Source	SS	df	MS	F	Prob > F
Columns	3.79E-05	4	9.46E-06	4.27E+01	4.53E-33
Error	2.22E-04	1000	2.22E-07		
Total	2.60E-04	1004			

Table E.3 shows the One-Way ANOVA results for the 7.33 m/s wind speed:

Table E.3: One-Way ANOVA, wind speed 7.33 m/s

Source	SS	df	MS	F	Prob > F
Columns	4.08E-05	4	1.02E-05	3.08E+00	1.56E-02
Error	3.32E-03	1000	3.32E-06		
Total	3.36E-03	1004			

E.0.12 Mean Multiple Comparison Test

Table E.4 shows the Multiple Comparison Test results for the 0.89 m/s wind speed:

Table E.4: Mean Multiple Comparison Test, wind speed 0.89 m/s

Sample	Sample	CI Lower	Mean Δ	CI Upper	Significant
1	2	3.17E-05	1.55E-04	2.77E-04	Significant
1	3	1.34E-04	2.57E-04	3.80E-04	Significant
2	3	-2.05E-05	1.02E-04	2.25E-04	Not Significant

Table E.5 shows the Multiple Comparison Test results for the 4.11 m/s wind speed:

Table E.5: Mean Multiple Comparison Test, wind speed 4.11 m/s

Sample	Sample	CI Lower	Mean Δ	CI Upper	Significant
1	2	-1.84E-04	-5.63E-05	7.19E-05	Not Significant
1	3	-1.59E-04	-3.10E-05	9.71E-05	Not Significant
1	4	-4.92E-04	-3.63E-04	-2.35E-04	Significant
1	5	-5.99E-04	-4.71E-04	-3.43E-043	Significant
2	3	-1.03E-04	2.53E-05	1.53E-04	Not Significant
2	4	-4.35E-04	-3.07E-04	-1.79E-04	Significant
2	5	-5.43E-04	-4.15E-04	-2.87E-04	Significant
3	4	-4.61E-04	-3.32E-04	-2.04E-04	Significant
3	5	-5.68E-04	-4.40E-04	-3.12E-04	Significant
4	5	-2.36E-04	-1.08E-04	2.03E-05	Not Significant

Table E.6 shows the Multiple Comparison Test results for the 7.33 m/s wind speed:

Table E.6: Mean Multiple Comparison Test, wind speed 7.33 m/s

Sample	Sample	CI Lower	Mean Δ	CI Upper	Significant
1	2	-7.90E-04	-2.95E-04	2.01E-04	Not Significant
1	3	-8.99E-04	-4.04E-04	9.21E-05	Not Significant
1	4	-9.06E-04	-4.10E-04	8.55E-05	Not Significant
1	5	-1.11E-03	-6.17E-04	-1.21E-043	Significant
2	3	-6.04E-04	-1.09E-04	3.87E-04	Not Significant
2	4	-6.11E-04	-1.16E-04	3.80E-04	Not Significant
2	5	-8.18E-04	-3.22E-04	1.73E-04	Not Significant
3	4	-5.02E-04	-6.63E-06	4.89E-04E-04	Not Significant
3	5	-7.09E-04	-2.13E-04	2.82E-04	Not Significant
4	5	-7.02E-04	-2.07E-04	2.89E-04	Not Significant

E.0.13 Kruskal-Wallis Test

Table E.7 shows the Kruskal-Wallis Test results for the 0.89 m/s wind speed:

Table E.7: Kruskal-Wallis Test, wind speed 0.89 m/s

Source	SS	df	MS	Chi-sq	Prob > Chi-sq
Columns	1.79E+05	2	8.97E+04	5.91E+00	5.20E-02
Error	1.81E+07	600	3.02E+04		
Total	1.83E+07	602			

Table E.8 shows the Kruskal-Wallis Test results for the 4.11 m/s wind speed:

Table E.8: Kruskal-Wallis Test, wind speed 4.11 m/s

Source	SS	df	MS	Chi-sq	Prob > Chi-sq
Columns	1.04E+07	4	2.60E+06	1.23E+02	9.92E-26
Error	7.42E+07	1000	7.42E+04		
Total	8.46E+07	1004			

Table E.9 shows the Kruskal-Wallis Test results for the 7.33 m/s wind speed:

Table E.9: Kruskal-Wallis Test, wind speed 7.33 m/s

Source	SS	df	MS	Chi-sq	Prob > Chi-sq
Columns	3.90E+06	4	9.76E+05	4.63E+01	2.11E-09
Error	8.07E+07	1000	8.07E+04		
Total	8.46E+07	1004			

E.0.14 Median Multiple Comparison Test

Table E.10 shows the Multiple Comparison Test results for the 0.89 m/s wind speed:

Table E.10: Median Multiple Comparison Test, wind speed 0.89 m/s

Sample	Sample	CI Lower	Median Δ	CI Upper	Significant
1	2	-2.44E+01	1.63E+01	5.71E+01	Not Significant
1	3	-6.63E+01	-2.56E+01	1.52E+01	Not Significant
2	3	-8.26E+01	-4.19E+01	-1.19E+00	Significant

Table E.11 shows the Multiple Comparison Test results for the 4.11 m/s wind speed:

Table E.11: Median Multiple Comparison Test, wind speed 4.11 m/s

Sample	Sample	CI Lower	Median Δ	CI Upper	Significant
1	2	-1.01E+02	-2.17E+01	5.73E+01	Not Significant
1	3	-9.11E+01	-1.21E+01	6.69E+01	Not Significant
1	4	-2.84E+02	-2.05E+02	-1.26E+02	Significant
1	5	-3.10E+02	-2.31E+02	-1.52E+02	Significant
2	3	-6.94E+01	9.56E+00	8.85E+01	Not Significant
2	4	-2.62E+02	-1.83E+02	-1.04E+02	Significant
2	5	-2.88E+02	-2.09E+02	-1.30E+02	Significant
3	4	-2.71E+02	-1.92E+02	-1.13E+02	Significant
3	5	-2.98E+02	-2.19E+02	-1.40E+02	Significant
4	5	-1.05E+02	-2.64E+01	5.26E+01	Not Significant

Table E.12 shows the Multiple Comparison Test results for the 7.33 m/s wind speed:

Table E.12: Median Multiple Comparison Test, wind speed 7.33 m/s

Sample	Sample	CI Lower	Median Δ	CI Upper	Significant
1	2	-2.30E+02	-1.51E+02	-7.21E+01	Significant
1	3	-2.30E+02	-1.51E+02	-7.23E+01	Significant
1	4	-2.25E+02	-1.46E+02	-6.75E+01	Significant
1	5	-2.48E+02	-1.69E+02	-9.04E+01	Significant
2	3	-7.92E+01	-1.84E-01	7.88E+01	Not Significant
2	4	-7.43E+01	4.66E+00	8.36E+01	Not Significant
2	5	-9.72E+01	-1.82E+01	6.07E+01	Not Significant
3	4	-7.41E+01	4.84E+00	8.38E+01	Not Significant
3	5	-9.70E+01	-1.81E+01	6.09E+01	Not Significant
4	5	-1.02E+02	-2.29E+01	5.61E+01	Not Significant

Appendix F

Matlab Sample Scripts

F.0.15 Introduction

Appendix D contains Sample Matlab Scripts used for post-processing the Fluent Data.

F.0.16 Contour Phase Plots

The script is presented below. ContourPlotPhase5.m

```
% File: ContourPlotPhase5.m
% Purpose: Plots Contours of Volume Fraction of Air
% over domain 5 to 10 m from inlet of tank
% Author: Edward Greig ENG4111/2 2012
% Input: *.xls [ x position from inlet (m) (ordered 10 down to 5 m),
% Volume Fraction of Air (order 0 down to 0.850 m for each x position)]
% Note: CFD domain is -15 m to 0 m, inlet to outlet.
% Output: Contour plot of volume fraction of air identifying interface
% waves
%
% Clear Variables and Command Window
clear;clc;
% Prompt user for file in correct format e.g. 733_8s_phase.xls
filename = uigetfile
% Pass selected file through xlsread and assign to P variable
P = xlsread(filename);
% Note size of P and G, inspect to see if match original spreadsheet
F = size(P), G = F(1,1)/36    % should be [7236 2] & [201]
% Extract first 36 lines of variable in column 2 (phase)
% and insert into column 1 of matrix z. Repeat next 36 lines, insert
% column 2,
% and build matrix from 10 m L to 5 m R
% Note: water is above air in matrix and image is reversed 10 to 5 m
% not 5 to 10 m
```

```
z(1:36,1)=P(1:36,2);
for k=1:200
    % increment k for new column
    k=k+1;
z(1:36,k)=P(((36*(k-1))+1):(36*k),2);
end
% The air/water interface is included twice in data, remove line 19
% (same as 18).
% B is matrix with line 19 removed.
B = [z(1:18,:);z(20:36,:)];
% set x limits, distance from inlet
x = [5:0.025:10]; size(x);
% set y limits, vertical tank distance from floor
y = [0:0.025:0.85]; size(y);
% generate index matrices for x and y, to be coupled with B i.e.
% (i,j,k in 3D)
[x,y]=meshgrid(x,y);
% Extract Screen Size
fullscreen = get(0,'ScreenSize');
% Set plot output to screen size.
figure('Position',[0 0 fullscreen(3) fullscreen(4)]);
% compute filled contour plot, 12 contour lines specified
[c,h] = contourf(x,y,B,12,'EdgeColor','none') % <- General contour
% function use suggested by A.Wandel. Contourf by Edward Greig.
% Plotting with contourf orients air/water and 5-10 m in the correct order.
% Verified against volume fraction images from ANSYS Fluent.
%
% The volume fraction colorbar, see below, indicates volume
% fraction is correctly oriented as well. 1 for air phase.
% 0 for water phase.
%
% Graph Appearance modificatons
axis equal     % <- Suggested by A.Wandel, change aspect to be equal
```

```
% x-axis label
xlabel('Distance from Inlet (m)','Interpreter','LaTex','FontSize',24)
% y-axis label
ylabel('Distance from Floor (m)','Interpreter','LaTex','FontSize',24)
% set axis font size
set(gca,'FontSize',20)
% set axis font
set(gca, 'FontName', 'Helvetica')
% use colour bar for label
ylabel(colorbar,'Volume Fraction of Air','Interpreter','LaTex',...
    'FontSize',24)
set(gca,'FontSize',20)
% set colour bar limits
set(gca, 'CLim', [0,1]);
% set correct x axis tick labels
set(gca,'XTickLabel',[5:0.5:10])
% modify y axis tick spacing
set(gca,'YTick',[0:0.425:0.85])
% set y-axis tick labels
set(gca,'YTickLabel',[0.00:0.425:0.85])
%
% EOF
```

F.0.17 Contour Horizontal Velocity Gradient Plots

The script is presented below. ContourVelGradient2.m

```
% File: ContourVelGradient2.m
% Purpose: Plots Contours of Horizontal Velocity Gradient
% over domain 5 to 10 m from inlet of tank
% Author: Edward Greig ENG4111/2 2012
% Input: *.xls [ x position from inlet (m) (ordered 10 down to 5 m),
% Horizontal Vel Gradient (order 0 down to 0.850 m for each x position)]
% Note: CFD domain is -15 m to 0 m, inlet to outlet.
% Output: Contour plot of horizontal velocity gradient
% identifying interface waves
%
% Clear Variables and Command Window
clear;clc;
% Prompt user for file in correct format e.g. 733_8s_vel.xls
filename = uigetfile
% Pass selected file through xlsread and assign to P variable
P = xlsread(filename);
% Note size of P and G, inspect to see if match original spreadsheet
F = size(P), G = F(1,1)/36    % should be [7236 2] & [201]
% Extract first 36 lines of variable in column 2 (Horizontal Vel Gradient)
% and insert into column 1 of matrix z. Repeat next 36 lines, insert
% column 2,
% and build matrix from 10 m L to 5 m R
% Note: water is above air in matrix and image is reversed 10 to 5 m
% not 5 to 10 m
z(1:36,1)=P(1:36,2);
for k=1:200
    % increment k for new column
    k=k+1;
z(1:36,k)=P(((36*(k-1))+1):(36*k),2);
```

```
end
% The air/water interface is included twice in data, remove line 19
% (same as 18).
% B is matrix with line 19 removed.
B = [z(1:18,:);z(20:36,:)];
% set x limits, distance from inlet
x = [5:0.025:10]; size(x);
% set y limits, vertical tank distance from floor
y = [0:0.025:0.85]; size(y);
% generate index matrices for x and y, to be coupled with B i.e.
% (i,j,k in 3D)
[x,y]=meshgrid(x,y);
% Extract Screen Size
fullscreen = get(0,'ScreenSize');
% Set plot output to screen size.
figure('Position',[0 0 fullscreen(3) fullscreen(4)]);
% compute filled contour plot, 20 contour lines specified
[c,h] = contourf(x,y,B,20,'EdgeColor','none') % <- General contour
% function use suggested by A.Wandel. Contourf by Edward Greig.
% Plotting with contourf orients air/water and 5-10 m in the correct order.
%
% Graph Appearance modificatons
axis equal     % <- Suggested by A.Wandel, change aspect to be equal
% x-axis label
xlabel('Distance from Inlet (m)','Interpreter','LaTex','FontSize',24)
% y-axis label
ylabel('Distance from Floor (m)','Interpreter','LaTex','FontSize',24)
% set axis font size
set(gca,'FontSize',20)
% set axis font
set(gca, 'FontName', 'Helvetica')
% use colour bar for label
ylabel(colorbar,...
```

```
'Horizontal Velocity Gradient $\frac{\partial{V}_{x}}{\partial{y}}$ (1/s)',...
'Interpreter','LaTex','FontSize',24)
set(gca,'FontSize',20)
% set colour bar limits
% set(gca, 'CLim', [0,1]); OFF
% set correct x axis tick labels
set(gca,'XTickLabel',[5:0.5:10])
% modify y axis tick spacing
set(gca,'YTick',[0:0.425:0.85])
% set y-axis tick labels
set(gca,'YTickLabel',[0.00:0.425:0.85])
%
% EOF
```

F.0.18 Shear Stress Distribution Plots

The 7.33 m/s script is presented below. Similar scripts were prepared for the 4.11 m/s and 0.89 m/s samples. Files: highdistplot.m, middistplot.m, lowdistplot.m

```
% File: highdistplot.m
% Purpose: Plots relative frequency distribution of sampled shear stresses
% Author: Edward Greig ENG4111/2 2012
% Input: 733dataRaw.xls [ x position from inlet (m), ...
% 2 s Shear Stress (Pa), 4 s Shear Stress, 6 s Shear Stress, ...
% 8 s Shear Stress, 10 s Shear Stress ]
% Output: Distribution plots per sampling time
%
% Clear variables and Command Window
clear;clc;
% Read Data File for 7.33 m/s Sample
A = xlsread('733dataRaw.xls');
% node location from tank inlet
NCol = A(:,1);
% 2 s Shear Stress
A2 = A(:,2);
% 4 s Shear Stress
A4 = A(:,3);
% 6 s Shear Stress
A6 = A(:,4);
% 8 s Shear Stress
A8 = A(:,5);
% 10 s Shear Stress
A10 = A(:,6);
%
% Generate frequency count and bin centre vectors, 20 bins ...
% over range of data
[nA2,xoutA2] = hist(A2,20);
```

```
[nA4,xoutA4] = hist(A4,20);
[nA6,xoutA6] = hist(A6,20);
[nA8,xoutA8] = hist(A8,20);
[nA10,xoutA10] = hist(A10,20);
%
% Extract Screen Size
fullscreen = get(0,'ScreenSize');
% Set plot output to screen size.
figure('Position',[0 0 fullscreen(3) fullscreen(4)]);

% Subplot Wind Speed 7.33 m/s t = 2 s
subplot(2,2,1)
% generate bar graph centred on xout with relative frequency
bar(xoutA2,nA2/sum(nA2),'k')
xlabel('Shear Stress (Pa)','Interpreter','LaTex','FontSize',24)
ylabel('Relative frequency $(\%)$','Interpreter','LaTex','FontSize',24)
title('t = 2.05 s','Interpreter','LaTex','FontSize',24)
%ylim([0 0.3])
%xlim([-0.00009 0.0008])
set(gca,'FontSize',20)
set(gca, 'FontName', 'Helvetica')
grid on
%
% Subplot Wind Speed 7.33 m/s t = 4 s
subplot(2,2,2)
bar(xoutA4,nA4/sum(nA4),'k')
xlabel('Shear Stress (Pa)','Interpreter','LaTex','FontSize',24)
ylabel('Relative frequency $(\%)$','Interpreter','LaTex','FontSize',24)
title('t = 4.10 s','Interpreter','LaTex','FontSize',24)
%ylim([0 0.3])
%xlim([-0.010 0.005])
set(gca,'FontSize',20)
set(gca, 'FontName', 'Helvetica')
```

```
grid on
%
% Subplot Wind Speed 7.33 m/s t = 6 s
subplot(2,2,3)
bar(xoutA6,nA6/sum(nA6),'k')
xlabel('Shear Stress (Pa)','Interpreter','LaTex','FontSize',24)
ylabel('Relative frequency $(\%)$','Interpreter','LaTex','FontSize',24)
title('t = 6.15 s','Interpreter','LaTex','FontSize',24)
%ylim([0 0.3])
%xlim([-0.010 0.005])
set(gca,'FontSize',20)
set(gca, 'FontName', 'Helvetica')
grid on
%
% Subplot Wind Speed 7.33 m/s t = 8 s
subplot(2,2,4)
bar(xoutA8,nA8/sum(nA8),'k')
xlabel('Shear Stress (Pa)','Interpreter','LaTex','FontSize',24)
ylabel('Relative frequency $(\%)$','Interpreter','LaTex','FontSize',24)
title('t = 8.20 s','Interpreter','LaTex','FontSize',24)
%ylim([0 0.3])
%xlim([-0.010 0.005])
set(gca,'FontSize',20)
set(gca, 'FontName', 'Helvetica')
grid on
%
% Subplot Wind Speed 7.33 m/s t = 10 s
%subplot(2,3,5)
%bar(xoutA10,nA10/sum(nA10),'k')
xlabel('Shear Stress (Pa)','Interpreter','LaTex','FontSize',24)
ylabel('Relative frequency $(\%)$','Interpreter','LaTex','FontSize',24)
title('t = 10.6 s','Interpreter','LaTex','FontSize',24)
%ylim([0 0.3])
```

```
%xlim([-0.010 0.005])
set(gca,'FontSize',20)
set(gca, 'FontName', 'Helvetica')
grid on
%
% EOF
```

F.0.19 Sample Shear Stress Profile Plots

The 7.33 m/s script is presented below. Similar scripts were prepared for the 4.11 m/s and 0.89 m/s samples. Files: highshearprofile.m, midshearprofile.m, lowshearprofile.m

```
% File: highshearprofile.m
% Purpose: Plots the 7.33 m/s shear stress at each node beyween 5 and 10 m
% according to the filtering method.
% Author: Edward Greig ENG4111/2 2012
% Input: 733dataRaw.xls [ x position from inlet (m), ...
% 2 s Shear Stress (Pa), 4 s Shear Stress, 6 s Shear Stress, ...
% 8 s Shear Stress, 10 s Shear Stress ]
% Output: Shear Stress Plot with position from inlet.
%
% Clear variables and Command Window
clear;clc;
% Read Data File for 4.11 m/s Sample
A = xlsread('733dataRaw.xls');
% node location from tank inlet
NCol = A(:,1);
% 2 s Shear Stress
A2 = A(:,2);
% 4 s Shear Stress
A4 = A(:,3);
% 6 s Shear Stress
A6 = A(:,4);
% 8 s Shear Stress
A8 = A(:,5);
% 10 s Shear Stress
A10 = A(:,6);
%
% Extract Screen Size
fullscreen = get(0,'ScreenSize');
```

```
% Set plot output to screen size.
figure('Position',[0 0 fullscreen(3) fullscreen(4)]);


hold on
% Subplot for 2 s Sample
subplot(5,1,1)
plot(NCol,A2,'k')
set(gca,'FontSize',20)
grid on
%ylabel('Instantaneous Shear Stress (Pa)','FontSize',16)
xlabel('','FontSize',24)
title('2.05 s','Interpreter','LaTex','FontSize',24)
set(gca,'FontSize',20)
set(gca, 'FontName', 'Helvetica')
grid on
% Subplot for 4 s Sample
subplot(5,1,2)
plot(NCol,A4,'k')
set(gca,'FontSize',20)
grid on
%ylabel('       Instantaneous Shear Stress (Pa)','FontSize',16)
xlabel('','FontSize',24)
title('4.10 s','Interpreter','LaTex','FontSize',24)
set(gca,'FontSize',20)
set(gca, 'FontName', 'Helvetica')
grid on
% Subplot for 6 s Sample
subplot(5,1,3)
plot(NCol,A6,'k')
set(gca,'FontSize',20)
grid on
ylabel('Sample Instantaneous Shear Stress (Pa)',...
    'Interpreter','LaTex','FontSize',24)
```

```
%xlabel('Distance from Inlet (m)','FontSize',16)
title('6.15 s','Interpreter','LaTex','FontSize',24)
set(gca,'FontSize',20)
set(gca, 'FontName', 'Helvetica')
grid on
% Subplot for 8 s Sample
subplot(5,1,4)
plot(NCol,A8,'k')
set(gca,'FontSize',20)
grid on
%ylabel('Instantaneous Shear Stress (Pa)','FontSize',16)
%xlabel('Distance from Inlet (m)','FontSize',16)
title('8.20 s','Interpreter','LaTex','FontSize',24)
set(gca,'FontSize',20)
set(gca, 'FontName', 'Helvetica')
grid on
% Subplot for 10 s Sample
subplot(5,1,5)
plot(NCol,A10,'k')
set(gca,'FontSize',20)
grid on
%ylabel('Instantaneous Shear Stress (Pa)','FontSize',16)
xlabel('Distance from Inlet (m)','Interpreter','LaTex','FontSize',24)
title('10.6 s','Interpreter','LaTex','FontSize',24)
set(gca,'FontSize',20)
set(gca, 'FontName', 'Helvetica')
grid on
%
% EOF
```

F.0.20 Sample Mean, Median and Standard Deviation

The sample mean plot script is presented below. Similar scripts were prepared for the median and standard deviation, with a variation to the function called. Files: allsamplemeanplot.m, allsamplemedianplot2.m, allsamplestdplot2.m

```
% File: allsamplemeanplot.m
% Purpose: Plots the mean of all samples vs normalised sample time
% Author: Edward Greig ENG4111/2 2012
% Input: 089dataRaw.xls, 411dataRaw.xls, 733dataRaw.xls [as defined in ...
% ANOVA and KW scripts]
% Output: Mean Shear Stress vs Normalised Sample Time
%
% Clear variables and Command Window
clear;clc;
% Read Data File for 0.89 m/s Sample
A = xlsread('089dataRaw.xls');
% node column location
NCol = A(:,1);
%17 s Shear Stress
A17 = A(:,2);
% 34 s Shear Stress
A34 = A(:,3);
% 51 s Shear Stress
A51 = A(:,4);
%
% Compute means
M1 = mean([A17 A34 A51])
%
% Sample Times
T1 = [0, 17,34,51];
% Residence time
R1 = 15/0.89;
```

```
% Normalised sample times
N1 = (1/R1)*T1;
%
% Read Data File for 4.11 m/s Sample
B = xlsread('411dataRaw.xls');
% node column location
NCol = B(:,1);
% 3 s Shear Stress
B3 = B(:,2);
% 7 s Shear Stress
B7 = B(:,3);
% 11 s Shear Stress
B11 = B(:,4);
% 14 s Shear Stress
B14 = B(:,5);
% 18 s Shear Stress
B18 = B(:,6);
% Compute means
M2 = mean([B3 B7 B11 B14 B18])
%
% Sample Times
T2 = [0, 3.65,7.31,11.0,14.6,18.8];
% Residence time
R2 = 15/4.11;
% Normalised sample times
N2 = (1/R2)*T2;
%
% Read Data File for 7.33 m/s Sample
D = xlsread('733dataRaw.xls');
% node column location
NCol = D(:,1);
% 2 s Shear Stress
D2 = D(:,2);
```

```
% 4 s Shear Stress
D4 = D(:,3);
% 6 s Shear Stress
D6 = D(:,4);
% 8 s Shear Stress
D8 = D(:,5);
% 10 s Shear Stress
D10 = D(:,6);
% Compute means
M3 = mean([D2 D4 D6 D8 D10])
%
% Sample Times
T3 = [0, 2.05,4.1,6.15,8.2,10.6];
% Residence time
R3 = 15/7.33;
% Normalised sample times
N3 = (1/R3)*T3;
%
% Generate matrix of means for plotting
one = [0 M1(1) M1(2) M1(3) 0 0 ]
fours = [0 M2(1) M2(2) M2(3) M2(4) M2(5)]
sevens = [ 0 M3(1) M3(2) M3(3) M3(4) M3(5)]
means = [ [0 1,2,3,4,5]' one' fours' sevens']
%
% Extract Screen Size
fullscreen = get(0,'ScreenSize');
% Set plot output to screen size.
figure('Position',[0 0 fullscreen(3) fullscreen(4)]);
%
hold on
% plot lines
plot(N1,means(1:4,2),'k','LineWidth',2)
plot(N2,means(1:6,3),'-r','LineWidth',5)
```

```
plot(N3,means(1:6,4),'-b','LineWidth',2)
% plot markers
plot(N1,means(1:4,2),'yd','MarkerSize',10,'MarkerFaceColor','k',...
    'MarkerEdgeColor','k')
plot(N2,means(1:6,3),'yd','MarkerSize',10,'MarkerFaceColor','k',...
    'MarkerEdgeColor','k')
plot(N3,means(1:6,4),'yd','MarkerSize',10,'MarkerFaceColor','k',...
    'MarkerEdgeColor','k')
% Graph Appearance
ylim([-0.0004 0.001])
xlabel('Normalised Sampling time   ${t}/{{t}_{res}}$','Interpreter'...
    ,'LaTex','FontSize',24)
ylabel('Shear Stress Sample Average (Pa)','Interpreter','LaTex','FontSize',24)
set(gca,'FontSize',20)
set(gca, 'FontName', 'Helvetica')
grid on
leg = legend('0.89 m/s','4.11 m/s','7.33 m/s')
%
 %EOF
```

F.0.21 One-Way ANOVA and Multiple Comparison Test

The 7.33 m/s script is presented below. Similar scripts were prepared for the 4.11 m/s and 0.89 m/s runs, with a variation to the input file and number of shear stress columns. Files: highrunANOVA.m, midrunANOVA.m, lowrunANOVA.m

```
% File: highrunANOVA.m
% Purpose: Completes One-Way ANOVA and Multiple Comparison Test ...
% on 7.33 m/s sample
% Author: Edward Greig ENG4111/2 2012
% Input: 733dataRaw.xls [ x position from inlet (m), ...
% 2 s Shear Stress (Pa), 4 s Shear Stress, 6 s Shear Stress, ...
% 8 s Shear Stress, 10 s Shear Stress ]
% Output: ANOVA Table and Multiple Comparisons Table and Graph
%
% Clear variables and Command Window
clear;clc;
% Read Data File for 7.33 m/s Sample
A = xlsread('733dataRaw.xls');
% node column location
NCol = A(:,1);
% 2 s Shear Stress
A2 = A(:,2);
% 4 s Shear Stress
A4 = A(:,3);
% 6 s Shear Stress
A6 = A(:,4);
% 8 s Shear Stress
A8 = A(:,5);
% 10 s Shear Stress
A10 = A(:,6);
% Compute means
M = mean([A2 A4 A6 A8 A10])
```

```
%
% Matrix of columns for ANOVA analysis
C = [A2 A4 A6 A8 A10];
%
% Run one-way ANOVA Test
[p1,table1,stats1] = anova1(C)
%
% Run Multiple Comparison Test
% Default significance level 0.05
[c1,m1,h1,nms1] = multcompare(stats1)
%
% EOF
```

F.0.22 Kruskal-Wallis Test and Multiple Comparison Test

The 7.33 m/s script is presented below. Similar scripts were prepared for the 4.11 m/s and 0.89 m/s runs, with a variation to the input file and number of shear stress columns. Files: highrunKW.m, midrunKW.m, lowrunKW.m

```
% File: highrunKW.m
% Purpose: Completes Kruskal-Wallis Test and Multiple Comparison Test ...
% on 7.33 m/s sample
% Author: Edward Greig ENG4111/2 2012
% Input: 733dataRaw.xls [ x position from inlet (m), ...
% 2 s Shear Stress (Pa), 4 s Shear Stress, 6 s Shear Stress, ...
% 8 s Shear Stress, 10 s Shear Stress ]
% Output: Table and Multiple Comparisons Table and Graph
%
% Clear variables and Command Window
clear;clc;
% Read Data File for 7.33 m/s Sample
A = xlsread('733dataRaw.xls');
% node column location
NCol = A(:,1);
% 2 s Shear Stress
A2 = A(:,2);
% 4 s Shear Stress
A4 = A(:,3);
% 6 s Shear Stress
A6 = A(:,4);
% 8 s Shear Stress
A8 = A(:,5);
% 10 s Shear Stress
A10 = A(:,6);
% Compute means
M = mean([A2 A4 A6 A8 A10])
```

```
%
% Matrix of columns for KW analysis
C = [A2 A4 A6 A8 A10];
%
% Run KW Test
[p1,table1,stats1] = kruskalwallis(C)
%
% Run Multiple Comparison Test
% Default significance level 0.05
[c1,m1,h1,nms1] = multcompare(stats1)
%
% EOF
```

F.0.23 Aggregated Non-Significant Shear Stress vs. Wind Speed

The script is presented below. Windspeedmeanshear1.m

```
% File: Windspeedmeanshear1.m
% Purpose: Plots the mean of aggregated high non-significant samples ...
% vs Wind Speed
% Author: Edward Greig ENG4111/2 2012
% Input: 089dataRaw.xls, 411dataRaw.xls, 733dataRaw.xls [as defined in ...
% ANOVA and KW scripts]
% Output: Mean non-significant Shear Stress vs Wind speed (m/s)
%
% Clear variables and Command Window
clear;clc;
% Read Data File for 0.89 m/s Sample
A = xlsread('089dataRaw.xls');
% node column location
NCol = A(:,1);
%17 s Shear Stress
A17 = A(:,2);
% 34 s Shear Stress
A34 = A(:,3);
% 51 s Shear Stress
A51 = A(:,4);
%
% Aggregate higher non-significant means
P1 = [A34; A51];
% Compute mean
M1 = mean(P1)
%
% Read Data File for 4.11 m/s Sample
B = xlsread('411dataRaw.xls');
% node column location
```

```
NCol = B(:,1);
% 3 s Shear Stress
B3 = B(:,2);
% 7 s Shear Stress
B7 = B(:,3);
% 11 s Shear Stress
B11 = B(:,4);
% 14 s Shear Stress
B14 = B(:,5);
% 18 s Shear Stress
B18 = B(:,6);
% Aggregate higher non-significant means
P2 = [B14; B18];
% Compute mean
M2 = mean(P2)
%
% Read Data File for 7.33 m/s Sample
D = xlsread('733dataRaw.xls');
% node column location
NCol = D(:,1);
% 2 s Shear Stress
D2 = D(:,2);
% 4 s Shear Stress
D4 = D(:,3);
% 6 s Shear Stress
D6 = D(:,4);
% 8 s Shear Stress
D8 = D(:,5);
% 10 s Shear Stress
D10 = D(:,6);
% Aggregate higher non-significant means
P3 = [D4; D6; D8; D10];
% Compute mean
```

```
M3 = mean(P3)
%
% Plot vectors - zero used for lower boundary
x = [0, 0 ,M2, M3]
y = [0, 0.89 , 4.11, 7.33]
%
% Extract Screen Size
fullscreen = get(0,'ScreenSize');
% Set plot output to screen size.
figure('Position',[0 0 fullscreen(3) fullscreen(4)]);
%
hold on
% plot lines
plot(y,x,'-b','LineWidth',2)
% plot markers
plot(y,x,'yd','MarkerSize',10,'MarkerFaceColor','k',...
    'MarkerEdgeColor','k')
% Graph Appearance
%ylim([-0.0004 0.001])
ylabel('Aggregated Sample Mean Shear Stress (Pa)','Interpreter'...
    ,'LaTex','FontSize',24)
xlabel('Wind Speed (m/s)','Interpreter','LaTex','FontSize',24)
set(gca,'FontSize',20)
set(gca, 'FontName', 'Helvetica')
grid on
%
% EOF
```